Polarisations of the Z and W bosons in the processes $pp \to ZH$ and $pp \to W^\pm H$

Junya Nakamura

Institut für theoretische Physik, Universität Tübingen, Germany junya.nakamura@itp.uni-tuebingen.de

Abstract

The Z boson in the process $pp \to ZH$ and the W^+ and W^- in the process $pp \to W^\pm H$ can be in polarised states. The polarisation density matrix of the Z(W) boson contains the complete information about a state of polarisation of the Z(W) boson, and HZZ, $HZ\gamma$ and HWW interactions may be studied in detail from a careful analysis of these matrices. In this paper, a systematic approach to analyse these polarisation density matrices is presented. With the aim of making maximum use of the polarisation information, all of the elements of the polarisation density matrices are related with observables, which are measurable at the environment of pp collisions. Consequences of non-standard HZZ, $HZ\gamma$ and HWW interactions for these observables are discussed.

Contents

1	Introduction	2					
2	Constituents of the polarisation density matrices						
	2.1 Effective Lagrangian with CP -odd operators	3					
	2.2 Helicity amplitudes						
	2.3 Requests from symmetries	6					
3	Polarisation of the Z boson	7					
	3.1 Polarisation density matrices of the Z boson	7					
	3.2 Decay angular distributions of the polarised Z boson						
	3.3 Influences of non-standard HZZ and $HZ\gamma$ interactions						
4	Polarisation of the W boson	17					
	4.1 Polarisation density matrices of the W^+ and W^-	17					
	4.2 Decay angular distributions of the polarised W^+ and W^-	18					
	4.3 Influences of non-standard HWW interaction	20					
5	Summary	21					

1 Introduction

The ATLAS and CMS collaborations have observed the Higgs boson [1,2]. The measurements of the Higgs boson couplings to the standard model (SM) particles are essential tests of the SM. The Higgs boson couplings to the weak bosons, HZZ and HWW, can be measured by studying the production cross sections times branching fractions [3], by studying the angular distribution in the decay processes $H \to ZZ^* \to 4l$ and $H \to WW^* \to l\nu l\nu$ [4–12] and by studying kinematics of the production processes for instance the jet azimuthal angle correlation in the weak boson fusion production [10,13–16]. The ATLAS and CMS collaborations have already performed measurements of HZZ and HWW interactions by using the above three approaches in refs. [17–24], in refs. [22, 25–30] and in refs. [31–33], respectively. The production processes $pp \to ZH$ and $pp \to W^{\pm}H$ [34–46] provide direct access to the HZZ and HWW couplings, respectively. In these processes, not only the three approaches mentioned above, but also decay properties of the Z and W bosons can be used to study the HZZ and HWW interactions [47–55].

An arbitrary polarised state of a particle with spin s is entirely described by a $(2s+1) \times (2s+1)$ polarisation density matrix; see e.g. refs. [56–59]. When a particle with spin 1 is in an either completely or partially polarised state, it has 9 independent angular distributions of its decay products at its rest frame and the coefficients of these distributions are written in terms of all the elements of the polarisation density matrix; see e.g. refs. [58,59]. An experimental determination of the complete decay angular distributions of a particle's decay products is, therefore, identical to an attempt to determine the polarisation density matrix, from which detailed information in reactions which produce that particle can be extracted; see e.g. ref. [60] for a theoretical study and e.g. refs. [61–63] for experimental studies.

As the Z boson in the process $e^+e^- \to ZH$ can be in a polarised state [6,64–66], so the Z boson in the process $pp \to ZH$ can be. The W^+ and W^- in the process $pp \to W^\pm H$ can be also in polarised states. It would be, therefore, possible to study HZZ, $HZ\gamma$ and HWW interactions in detail from a careful analysis of these states of polarisation. As we mentioned in the previous paragraph, the polarisation density matrix of the Z(W) boson contains the complete information about a state of polarisation of the Z(W) boson. Hence all of the elements of the polarisation density matrix should be made use of in such a careful analysis. In this paper, we present a systematic approach to analyse the polarisation density matrices of the Z boson and W^\pm in the processes $pp \to ZH$ and $pp \to W^\pm H$. With the aim of making maximum use of the information about states of polarisation, we relate all of the elements of the polarisation density matrices with observables which we can measure at the environment of proton-proton (pp) collisions. We discuss consequences of non-standard HZZ, $HZ\gamma$ and HWW interactions for these observables. A detailed analysis of the polarisation of the Z boson in the process $e^+e^- \to ZH$ is present in

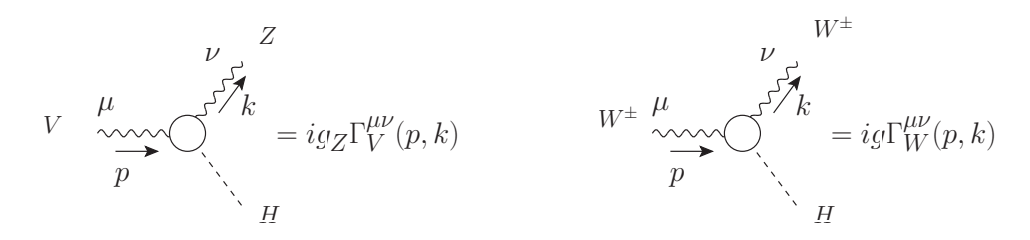


Figure 1: Feynman rules for the HZV $(V = Z, \gamma)$ vertex and the HWW vertex.

ref. [66]. Our approach in the process $pp \to ZH$ is an extension of that work to pp collisions.

The paper is organised as follows. In Section 2, we introduce all the ingredients needed for our analyses in the following sections. At first, we give non-standard HZZ, $HZ\gamma$ and HWW couplings. We present the complete helicity amplitudes for the sub-processes $q\bar{q} \to ZH$, $u\bar{d} \to W^+H$ and $d\bar{u} \to W^- H$. These amplitudes are given for the non-standard couplings. We derive the relations between the helicity amplitudes imposed by the CP and $CP\widetilde{T}$ symmetries. In Section 3, we analyse the polarisation density matrices of the Z boson in the process $pp \to ZH$ in detail. First of all, we define the polarisation density matrices consisting of the helicity amplitudes of the previous section. Then we derive the 4 different differential cross sections for the process $pp \to ZH$ followed by $Z \to f\bar{f}$ with respect to the Z decay angles. Among the 36 coefficients (= 9 × 4) of these 4 different differential angular distributions, only 15 coefficients can be non-zero. These coefficients are written in terms of the elements of the polarisation density matrices. The restrictions on these coefficients imposed by the CP and CPT symmetries are clarified. We focus on the coefficients which are strictly zero in the SM due to CP invariance or small in the SM due to the smallness of re-scattering effects, and study the influences of the non-standard HZZ and $HZ\gamma$ couplings. In Section 4, we analyse the polarisation density matrices of the W^+ and W^- in the process $pp \to W^{\pm}H$ following the same procedure as the previous section. Section 5 gives a summary.

2 Constituents of the polarisation density matrices

As the base vectors for the density matrices 1 , we choose the eigenfunctions of the helicity operator. The density matrices are, therefore, constructed of helicity amplitudes. In this section we derive the complete helicity amplitudes for the sub-processes $q\bar{q} \to ZH$, $u\bar{d} \to W^+H$ and $d\bar{u} \to W^-H$.

2.1 Effective Lagrangian with CP-odd operators

We derive non-standard HZZ, $HZ\gamma$ and HWW couplings from the following effective Lagrangian [66,67]:

$$\mathcal{L}_{\text{eff}} = \left(1 + a_Z\right) \frac{1}{2} g_Z m_Z H Z_\mu Z^\mu + \frac{g_Z}{2m_Z} \sum_{V = Z, \gamma} \left\{ b_V H Z_{\mu\nu} V^{\mu\nu} + c_V \left[(\partial^\mu H) Z^\nu - (\partial^\nu H) Z^\mu \right] V_{\mu\nu} \right. \\ \left. + \frac{1}{2} \tilde{b}_V \epsilon^{\mu\nu\rho\sigma} H Z_{\mu\nu} V_{\rho\sigma} \right\} \\ \left. + \left(1 + a_W\right) g m_W H W_\mu^\dagger W^\mu + \frac{g}{m_W} \left\{ b_W H W_{\mu\nu}^\dagger W^{\mu\nu} + c_W \left[(\partial_\mu H) W_\nu^\dagger W^{\mu\nu} - (\partial^\nu H) W^\mu W_{\mu\nu}^\dagger \right] \right. \\ \left. + \frac{1}{2} \tilde{b}_W \epsilon^{\mu\nu\rho\sigma} H W_{\mu\nu}^\dagger W_{\rho\sigma} \right\}, \tag{2.1}$$

where $V_{\mu\nu}=\partial_{\mu}V_{\nu}-\partial_{\nu}V_{\mu},\,W_{\mu\nu}=\partial_{\mu}W_{\nu}-\partial_{\nu}W_{\mu},\,W^{\mu}$ is the W^{-} field, $g=e/\sin\theta_{w},\,g_{Z}=g/\cos\theta_{w}$ with θ_{w} being the electroweak mixing angle and e being the proton charge, and $\epsilon_{0123}=+1$ in our convention. All of the eleven coefficients $a_{Z},\,a_{W},\,b_{V},\,c_{V}$ and $\tilde{b}_{V}\,(V=Z,\gamma,W)$ are real so that $\mathcal{L}_{\mathrm{eff}}=\mathcal{L}_{\mathrm{eff}}^{\dagger}$ and zero at the tree level in the SM. The operators whose coefficients are $a_{Z},\,a_{W},\,b_{V}$ and $c_{V}\,(V=Z,\gamma,W)$ are CP-even and the operators whose coefficients are $\tilde{b}_{V}\,(V=Z,\gamma,W)$ are CP-even operators indicates that H is a CP-even scalar field, while the Lagrangian with only the CP-odd operators indicates that H is a CP-odd scalar

¹Hereafter we call a polarisation density matrix a density matrix for short.

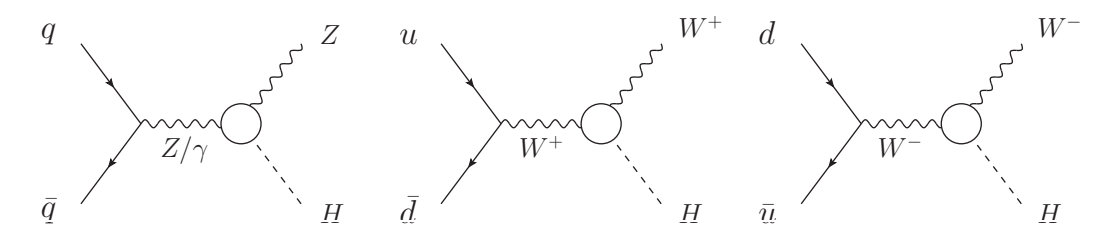


Figure 2: Feynman diagrams for the sub-processes $q\bar{q} \to ZH$, $u\bar{d} \to W^+H$ and $d\bar{u} \to W^-H$. The circles denote the non-standard couplings derived from the effective Lagrangian in eq. (2.1).

field. In both cases, the theory is CP invariant. If both the CP-even operator(s) and the CP-odd operator(s) exist, H is no longer a CP eigenstate and the theory is not CP invariant. We call a_Z , a_W , b_V and c_V ($V=Z,\gamma,W$) CP-even coefficients and \widetilde{b}_V ($V=Z,\gamma,W$) CP-odd coefficients.

If we assign the momenta as shown in Figure 1 2 , Feynman rules for the HZV $(V=Z,\gamma)$ vertex and the HWW vertex can be expressed as

$$\Gamma_{V}^{\mu\nu}(p,k) = m_{Z} \left(\delta_{ZV} + h_{1}^{V} + h_{2}^{V} \frac{\hat{s}}{m_{Z}^{2}} \right) g^{\mu\nu} + h_{3}^{V} \frac{k^{\mu} p^{\nu}}{m_{Z}} + \tilde{h}_{4}^{V} \epsilon^{\mu\nu\alpha\beta} \frac{p_{\alpha} k_{\beta}}{m_{Z}}, \tag{2.2a}$$

$$\Gamma_W^{\mu\nu}(p,k) = m_W \left(1 + h_1^W + h_2^W \frac{\hat{s}}{m_W^2} \right) g^{\mu\nu} + h_3^W \frac{k^\mu p^\nu}{m_W} + \widetilde{h}_4^W \epsilon^{\mu\nu\alpha\beta} \frac{p_\alpha k_\beta}{m_W}, \tag{2.2b}$$

where $\delta_{ZV}=1$ for V=Z, $\delta_{ZV}=0$ for $V=\gamma$, and $\hat{s}=(p)^2$. Terms proportional to k^ν vanish for the on-shell Z boson and the on-shell W boson, and terms proportional to p^μ also vanish in our processes where the intermediate off-shell vector boson (Z,γ) or W) couples to the four-vector consisting of the two massless quarks. These terms are, therefore, not included in the above formulae. All the form factors are constant and expressed in terms of the coefficients in the effective Lagrangian in eq. (2.1):

$$h_{1}^{Z} = a_{Z} + b_{Z} - (b_{Z} - c_{Z}) \frac{m_{H}^{2}}{m_{Z}^{2}}, \quad h_{1}^{\gamma} = \frac{1}{2} (b_{\gamma} - c_{\gamma}) \frac{m_{Z}^{2} - m_{H}^{2}}{m_{Z}^{2}}, \quad h_{1}^{W} = a_{W} + b_{W} - (b_{W} - c_{W}) \frac{m_{H}^{2}}{m_{W}^{2}},$$

$$h_{2}^{Z} = b_{Z}, \qquad h_{2}^{\gamma} = \frac{1}{2} (b_{\gamma} + c_{\gamma}), \qquad h_{2}^{W} = b_{W},$$

$$h_{3}^{Z} = -2(b_{Z} - c_{Z}), \qquad h_{3}^{\gamma} = -(b_{\gamma} - c_{\gamma}), \qquad h_{3}^{W} = -2(b_{W} - c_{W}),$$

$$\tilde{h}_{4}^{Z} = -2\tilde{b}_{Z}, \qquad \tilde{h}_{4}^{\gamma} = -\tilde{b}_{\gamma}, \qquad \tilde{h}_{4}^{W} = -2\tilde{b}_{W}. \qquad (2.3)$$

The form factors h_i^V $(V=Z,\gamma,W)$ (i=1,2,3) consist of the CP-even coefficients and \widetilde{h}_4^V $(V=Z,\gamma,W)$ consist of the CP-odd coefficients. We call h_i^V $(V=Z,\gamma,W)$ (i=1,2,3) CP-even form factors and \widetilde{h}_4^V $(V=Z,\gamma,W)$ CP-odd form factors.

2.2 Helicity amplitudes

Feynman diagrams for the sub-processes $q\bar{q}\to ZH,\,u\bar{d}\to W^+H$ and $d\bar{u}\to W^-H$ are shown in Figure 2. The circles denote the non-standard couplings derived in the previous section. We evaluate production helicity amplitudes in the following two frames. Let us assume that a direction of the z-axis is fixed along pp collisions. In one frame, which we call the $q\bar{q}^{(l)}$ centre-of-mass (c.m.) frame and is shown in the left picture of Figure 3, the quark (q) moves along the positive direction of the z-axis. In another frame, which we call the $q^{(l)}q$ c.m. frame and is shown in the right picture of Figure 3, the antiquark $(q^{(l)})$ moves along the positive direction of the z-axis. In Figure 3, our notation for helicities and the polar angle θ are also shown. We neglect the masses of q and $q^{(l)}$, thus the helicity of $q^{(l)}$ is always opposite to that of q in our sub-processes. Helicity amplitudes are, therefore, given for the quark helicity $\sigma(=\pm 1)$ and the weak boson helicity $\lambda(=\pm 1,0)$; the antiquark helicity is automatically fixed to $-\sigma^3$. We denote the helicity amplitudes evaluated in the $qq^{(l)}$ c.m. frame by $\mathcal{M}^{\lambda}_{\sigma}(qq^{(l)})$ and those evaluated in the $q^{(l)}q$ c.m. frame by $\mathcal{M}^{\lambda}_{\sigma}(qq^{(l)})$. It should be emphasised that σ always denotes the helicity of the quark and θ is the polar angle of the weak

²All pictures in this paper are drawn by using the program JaxoDraw [68].

³The fermion helicity is always normalised to ± 1 in this paper.

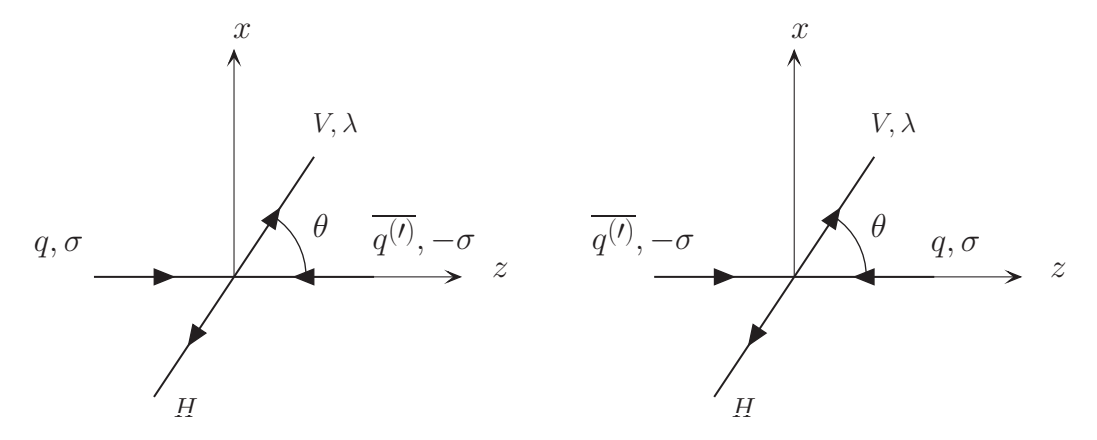


Figure 3: Left: the $q\overline{q^{(\prime)}}$ c.m. frame, where the quark (q) moves along the positive direction of the z-axis. The production amplitudes $\mathcal{M}^{\lambda}_{\sigma}(q\overline{q^{\prime}})$ are evaluated in this frame. Right: the $\overline{q^{(\prime)}}q$ c.m. frame, where the antiquark $(\overline{q^{(\prime)}})$ moves along the positive direction of the z-axis. The production amplitudes $\mathcal{M}^{\lambda}_{\sigma}(\overline{q^{\prime}}q)$ are evaluated in this frame. The quark helicity $\sigma(=\pm 1)$, the antiquark helicity $-\sigma$ and the weak boson helicity $\lambda(=\pm 1,0)$ are shown, and the polar angle θ of the weak boson V from the z-axis is denoted in both the frames

boson from the z-axis (not the quark momentum direction). The helicity amplitudes $\mathcal{M}_{\sigma}^{\lambda}(q\bar{q})$ for the sub-process $q\bar{q} \to ZH$ are

$$\mathcal{M}_{\sigma}^{\lambda=\pm}(q\bar{q}) = \sigma \frac{1 + \sigma\lambda\cos\theta}{\sqrt{2}}\hat{M}_{\sigma}^{\lambda=\pm},\tag{2.4a}$$

$$\mathcal{M}_{\sigma}^{\lambda=0}(q\bar{q}) = \sin\theta \hat{M}_{\sigma}^{\lambda=0}, \tag{2.4b}$$

where

$$\hat{M}_{\sigma}^{\lambda=\pm} = g_Z m_Z \sqrt{\hat{s}} \left[\frac{g_{Z\sigma}}{\hat{s} - m_Z^2} \left(1 + h_1^Z + h_2^Z \frac{\hat{s}}{m_Z^2} + i\lambda \tilde{h}_4^Z \frac{k\sqrt{\hat{s}}}{m_Z^2} \right) + \frac{Q_q e}{\hat{s}} \left(h_1^{\gamma} + h_2^{\gamma} \frac{\hat{s}}{m_Z^2} + i\lambda \tilde{h}_4^{\gamma} \frac{k\sqrt{\hat{s}}}{m_Z^2} \right) \right],$$

$$\hat{M}_{\sigma}^{\lambda=0} = -g_Z w \sqrt{\hat{s}} \left[\frac{g_{Z\sigma}}{\hat{s} - m_Z^2} \left(1 + h_1^Z + h_2^Z \frac{\hat{s}}{m_Z^2} + h_3^Z \frac{k^2 \sqrt{\hat{s}}}{m_Z^2 w} \right) + \frac{Q_q e}{\hat{s}} \left(h_1^{\gamma} + h_2^{\gamma} \frac{\hat{s}}{m_Z^2} + h_3^{\gamma} \frac{k^2 \sqrt{\hat{s}}}{m_Z^2 w} \right) \right].$$

$$(2.5)$$

Here $\sqrt{\hat{s}}$ is the $q\bar{q}$ c.m. energy, w is the energy of the Z boson: $w=(\hat{s}+m_Z^2-m_H^2)/(2\sqrt{\hat{s}}),$ k is the momentum of the Z boson: $k=\sqrt{w^2-m_Z^2},~Q_q$ is the electric charge of the quark in units of $e,~g_{Z+}=g_Z(-Q_q\sin^2\theta_w),$ and $g_{Z-}=g_Z(T_q^3-Q_q\sin^2\theta_w)$ where $T_u^3=1/2$ and $T_d^3=-1/2$.

Although the actual calculation of the helicity amplitudes $\mathcal{M}_{\sigma}^{\lambda}(\bar{q}q)$ is easy, it is also possible to estimate them from $\mathcal{M}_{\sigma}^{\lambda}(q\bar{q})$ as follows. If we denote the helicity of \bar{q} by σ and the helicity of q by $-\sigma$ (this is opposite to our helicity notation), the angular part is the same as $\mathcal{M}_{\sigma}^{\lambda}(q\bar{q})$ and the amplitudes are given by

$$\mathcal{M}^{\lambda=\pm}(\bar{q}(\sigma)q(-\sigma)) = \sigma \frac{1+\sigma\lambda\cos\theta}{\sqrt{2}}\hat{M}_{-\sigma}^{\lambda=\pm}, \tag{2.6a}$$

$$\mathcal{M}^{\lambda=0}(\bar{q}(\sigma)q(-\sigma)) = \sin\theta \hat{M}_{-\sigma}^{\lambda=0}, \tag{2.6b}$$

where the helicity of each particle is explicitly shown in parenthesis. Because the helicity of a quark is equal to its chirality and the helicity of an antiquark is opposite to its chirality in the massless limit, q with helicity $-\sigma$ has the chirality $-\sigma$. Hence the coupling $g_{Z\sigma}$ must be replaced by $g_{Z-\sigma}$ in eq. (2.5), and this replacement is expressed by $\hat{M}_{-\sigma}^{\lambda}$ in eq. (2.6). By the simple replacement $\sigma \to -\sigma$ in eq. (2.6), we obtain the helicity amplitudes $\mathcal{M}_{\sigma}^{\lambda}(\bar{q}q)$ in our helicity notation:

$$\mathcal{M}_{\sigma}^{\lambda=\pm}(\bar{q}q) = -\sigma \frac{1 - \sigma\lambda\cos\theta}{\sqrt{2}} \hat{M}_{\sigma}^{\lambda=\pm}, \tag{2.7a}$$

$$\mathcal{M}_{\sigma}^{\lambda=0}(\bar{q}q) = \sin\theta \hat{M}_{\sigma}^{\lambda=0}. \tag{2.7b}$$

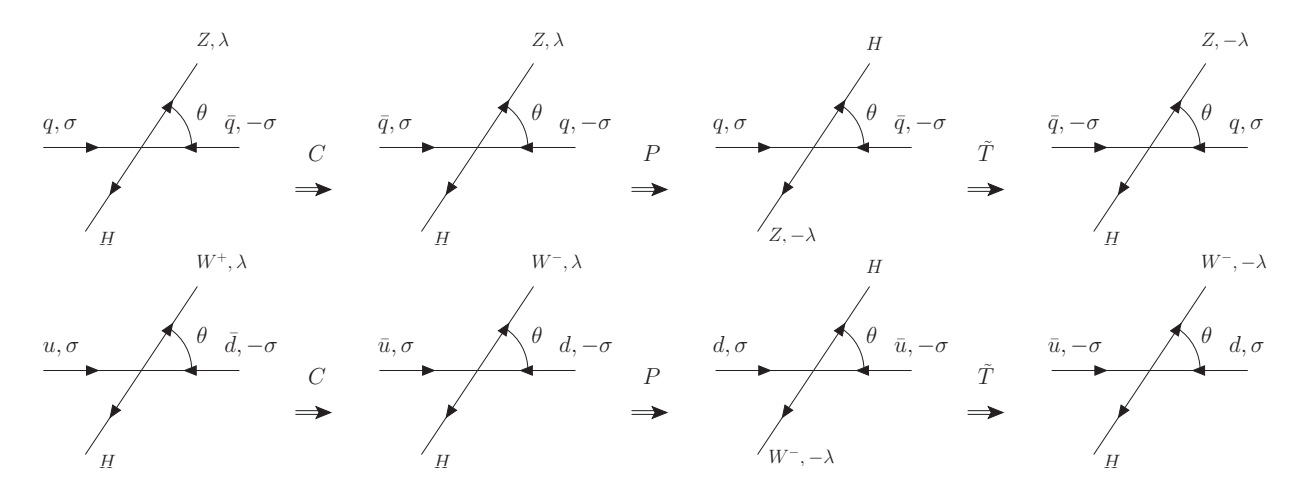


Figure 4: It is shown how the states in the process $q\bar{q} \to ZH$ (upper) and those in the process $u\bar{d} \to W^+H$ (lower) transform under C, P and T without interchanging the initial and final states (denoted by \tilde{T}).

We note that the relative sign among the amplitudes in eq. (2.4) and that among the amplitudes in eq. (2.7) are important, because they appear in the off-diagonal elements of the density matrices.

Similarly, the helicity amplitudes for the sub-process $u\bar{d} \to W^+H$ are given by

$$\mathcal{M}_{-}^{\lambda=\pm}(u\bar{d}) = -\frac{1-\lambda\cos\theta}{\sqrt{2}}(V_{ud})^* \hat{N}^{\lambda=\pm}, \tag{2.8a}$$

$$\mathcal{M}_{-}^{\lambda=0}(u\bar{d}) = \sin\theta \ (V_{ud})^* \ \hat{N}^{\lambda=0}, \tag{2.8b}$$

$$\mathcal{M}_{-}^{\lambda=\pm}(\bar{d}u) = \frac{1+\lambda\cos\theta}{\sqrt{2}}(V_{ud})^{*} \hat{N}^{\lambda=\pm}, \tag{2.8c}$$

$$\mathcal{M}_{-}^{\lambda=0}(\bar{d}u) = \sin\theta \ (V_{ud})^* \ \hat{N}^{\lambda=0}, \tag{2.8d}$$

and those for the sub-process $d\bar{u} \to W^- H$ are given by

$$\mathcal{M}_{-}^{\lambda=\pm}(d\bar{u}) = -\frac{1 - \lambda \cos \theta}{\sqrt{2}} V_{ud} \ \hat{N}^{\lambda=\pm}, \tag{2.9a}$$

$$\mathcal{M}_{-}^{\lambda=0}(d\bar{u}) = \sin\theta \ V_{ud} \ \hat{N}^{\lambda=0}, \tag{2.9b}$$

$$\mathcal{M}_{-}^{\lambda=\pm}(\bar{u}d) = \frac{1+\lambda\cos\theta}{\sqrt{2}}V_{ud}\hat{N}^{\lambda=\pm}, \tag{2.9c}$$

$$\mathcal{M}_{-}^{\lambda=0}(\bar{u}d) = \sin\theta \ V_{ud} \ \hat{N}^{\lambda=0}, \tag{2.9d}$$

where

$$\hat{N}^{\lambda=\pm} = \frac{1}{\sqrt{2}} g^2 m_W \sqrt{\hat{s}} \frac{1}{\hat{s} - m_W^2} \left(1 + h_1^W + h_2^W \frac{\hat{s}}{m_W^2} + i\lambda \tilde{h}_4^W \frac{k\sqrt{\hat{s}}}{m_W^2} \right),$$

$$\hat{N}^{\lambda=0} = -\frac{1}{\sqrt{2}} g^2 w \sqrt{\hat{s}} \frac{1}{\hat{s} - m_W^2} \left(1 + h_1^W + h_2^W \frac{\hat{s}}{m_W^2} + h_3^W \frac{k^2 \sqrt{\hat{s}}}{m_W^2 w} \right). \tag{2.10}$$

Here w is the energy of the W boson: $w=(\hat{s}+m_W^2-m_H^2)/(2\sqrt{\hat{s}}), k$ is the momentum of the W boson: $k=\sqrt{w^2-m_W^2}$, and V_{ud} is the element of the Cabibbo-Kobayashi-Maskawa (CKM) matrix.

By looking at the helicity amplitudes, we can already discuss a difference between the Z boson and the W boson with regard to states of polarisation. Since the W boson couples to only a fermion with chirality -1, the initial quark u or d always has the helicity $\sigma = -1$. Therefore, while the Z boson is in a partially polarised state (often called a mixed state; see e.g. refs. [56–59]), the W boson (both the W^+ and W^-) is in a completely polarised state (often called a pure state).

2.3 Requests from symmetries

Conditions imposed by symmetries lead to certain relations between the helicity amplitudes. The upper picture in Figure 4 shows how the states in the process $q\bar{q} \to ZH$ transform under C, P and

T without interchanging the initial and final states. By using a freedom of rotation around the z-axis after the C and P transformations, we find that the invariance under the CP transformation leads to the relation

$$\mathcal{M}_{\sigma}^{\lambda}(q\bar{q})(\theta) = \mathcal{M}_{\sigma}^{-\lambda}(q\bar{q})(\pi - \theta), \tag{2.11}$$

where $\mathcal{M}_{\sigma}^{\lambda}(q\bar{q})(\theta) = \mathcal{M}_{\sigma}^{\lambda}(q\bar{q})$ given in eq. (2.4), and $\mathcal{M}_{\sigma}^{-\lambda}(q\bar{q})(\pi-\theta)$ is obtained by setting $\theta \to \pi-\theta$ in $\mathcal{M}_{\sigma}^{-\lambda}(q\bar{q})$. It is easy to see that a non-zero value of the CP-odd form factors \tilde{h}_{4}^{Z} and/or \tilde{h}_{4}^{γ} violates this relation. Similarly, the lower picture in Figure 4 shows how the states in the process $u\bar{d} \to W^{+}H$ transform under C, P and T without interchanging the initial and final states. We find that CP invariance requests the relation

$$\mathcal{M}_{-}^{\lambda}(u\bar{d})(\theta) = \mathcal{M}_{-}^{-\lambda}(d\bar{u})(\pi - \theta), \tag{2.12}$$

where $\mathcal{M}_{-}^{\lambda}(u\bar{d})(\theta) = \mathcal{M}_{-}^{\lambda}(u\bar{d})$ given in eq. (2.8), and $\mathcal{M}_{-}^{-\lambda}(d\bar{u})(\pi-\theta)$ is obtained by setting $\theta \to \pi - \theta$ in $\mathcal{M}_{-}^{-\lambda}(d\bar{u})$ given in eq. (2.9). This relation is violated by the imaginary part of the element V_{ud} of the CKM matrix, even when the CP-odd form factor \tilde{h}_{4}^{W} is zero. However, this CP violation phase in V_{ud} [69] is always regarded as an overall common phase among the amplitudes. For instance, the phase in V_{ud} is an overall common phase among $\mathcal{M}_{-}^{\lambda=+}(d\bar{u})$, $\mathcal{M}_{-}^{\lambda=-}(d\bar{u})$ and $\mathcal{M}_{-}^{\lambda=0}(d\bar{u})$. Therefore, the effect of the CP violation phase in the CKM matrix never appears even in the off-diagonal elements of the density matrices. Only a non-zero value of the CP-odd form factor \tilde{h}_{4}^{W} violates the relation in eq. (2.12) and affects a state of polarisation of the W boson. We can write the relations in eqs. (2.11) and (2.12) in the following convenient forms, respectively:

$$\hat{M}_{\sigma}^{\lambda} = \hat{M}_{\sigma}^{-\lambda},\tag{2.13a}$$

$$\hat{N}^{\lambda} = \hat{N}^{-\lambda}.\tag{2.13b}$$

CPT invariance and the unitarity condition conclude [60] that the following relations 4 hold at the tree level approximation and violation of the relations indicates the existence of re-scattering effects:

$$\mathcal{M}_{\sigma}^{\lambda}(q\bar{q}) = -\left\{\mathcal{M}_{\sigma}^{-\lambda}(\bar{q}q)\right\}^{*},\tag{2.14a}$$

$$\mathcal{M}_{-}^{\lambda}(u\bar{d}) = -\left\{\mathcal{M}_{-}^{-\lambda}(\bar{u}d)\right\}^{*}.$$
(2.14b)

The amplitudes in the right hand side without complex conjugate can be read from the states after the $CP\widetilde{T}$ transformation in Figure 4. It is easy to see that the relations hold if all of the form factors are real. Following ref. [60], we call the invariance which leads to these relations $CP\widetilde{T}$ invariance. We can write the relations in eq. (2.14) in the following convenient forms, respectively:

$$\hat{M}_{\sigma}^{\lambda} = (\hat{M}_{\sigma}^{-\lambda})^*, \tag{2.15a}$$

$$\hat{N}^{\lambda} = (\hat{N}^{-\lambda})^*. \tag{2.15b}$$

3 Polarisation of the Z boson

3.1 Polarisation density matrices of the Z boson

In this section we define the density matrices of the Z boson by using our notation of the helicity amplitudes of the previous section. We consider the sub-process

$$q(\sigma) + \bar{q}(-\sigma) \to Z(\lambda) + H;$$

$$Z(\lambda) \to f(\tau) + \bar{f}(-\tau),$$
(3.1)

where the helicity of each particle is shown in parenthesis. We neglect the masses of the final fermion f and the final antifermion \bar{f} , thus the helicity of \bar{f} is always opposite to that of f. We express the full helicity amplitude as

$$\mathcal{T}_{\sigma}^{\tau}(q\bar{q}) = P_Z \sum_{\lambda = \pm, 0} \mathcal{M}_{\sigma}^{\lambda}(q\bar{q}) \ D_{\lambda}^{\tau}, \tag{3.2}$$

⁴Since the amplitude in the left hand side and the amplitude in the right hand side relate to the different reactions, interference between which is not possible, the minus sign in the right hand side (i.e. a relative phase) is not physical and solely due to our phase convention.

where the production amplitude $\mathcal{M}_{\sigma}^{\lambda}(q\bar{q})$ is given in eq. (2.4), D_{λ}^{τ} is the decay helicity amplitude, and

$$P_Z = (Q^2 - m_Z^2 + im_Z \Gamma_Z)^{-1}$$
(3.3)

denotes the propagator factor of the Z boson. We evaluate the decay amplitude in the following four-momentum frame:

$$Z: (m_{Z}, 0, 0, 0)$$

$$f: \frac{m_{Z}}{2} (1, \sin \widehat{\theta} \cos \widehat{\phi}, \sin \widehat{\theta} \sin \widehat{\phi}, \cos \widehat{\theta})$$

$$\bar{f}: \frac{m_{Z}}{2} (1, -\sin \widehat{\theta} \cos \widehat{\phi}, -\sin \widehat{\theta} \sin \widehat{\phi}, -\cos \widehat{\theta}).$$
(3.4)

The decay amplitude is

$$D_{\lambda}^{\tau} = g_{Zf\bar{f}}^{\tau} \ m_Z \ d_{\lambda}^{\tau}, \tag{3.5}$$

where

$$d_{\lambda=\pm}^{\tau} = \tau \frac{1 + \lambda \tau \cos \hat{\theta}}{\sqrt{2}} e^{i\lambda \hat{\phi}}, \tag{3.6a}$$

$$d_{\lambda=0}^{\tau} = \sin \widehat{\theta}. \tag{3.6b}$$

The explicit forms of the coupling $g_{Zf\bar{f}}^{\tau}$ are, $g_{Zl\bar{l}}^{+}=g_{Z}\sin^{2}\theta_{w}$ and $g_{Zl\bar{l}}^{-}=g_{Z}(-1/2+\sin^{2}\theta_{w})$ for a charged lepton pair, $g_{Zu\bar{u}}^{+}=-(2/3)g_{Z}\sin^{2}\theta_{w}$ and $g_{Zu\bar{u}}^{-}=g_{Z}(1/2-(2/3)\sin^{2}\theta_{w})$ for a up-type quark pair, $g_{Zd\bar{d}}^{+}=(1/3)g_{Z}\sin^{2}\theta_{w}$ and $g_{Zd\bar{d}}^{-}=g_{Z}(-1/2+(1/3)\sin^{2}\theta_{w})$ for a down-type quark pair. A straightforward manipulation gives

$$\sum_{\sigma} \left| \mathcal{T}_{\sigma}^{\tau}(q\bar{q}) \right|^{2} = \left| P_{Z} m_{Z} g_{Zf\bar{f}}^{\tau} \right|^{2} \sum_{\sigma} \sum_{\lambda',\lambda} \left(d_{\lambda'}^{\tau} \right)^{*} \rho_{\sigma}^{\lambda'\lambda}(q\bar{q}) d_{\lambda}^{\tau}
= \left| P_{Z} m_{Z} g_{Zf\bar{f}}^{\tau} \right|^{2} d^{\tau\dagger} \sum_{\sigma} \rho_{\sigma}(q\bar{q}) d^{\tau},$$
(3.7)

where

$$\sum_{\sigma} \rho_{\sigma}^{\lambda'\lambda}(q\bar{q}) = \sum_{\sigma} \{\mathcal{M}_{\sigma}^{\lambda'}(q\bar{q})\}^* \mathcal{M}_{\sigma}^{\lambda}(q\bar{q})$$
(3.8)

represents the elements of the density matrix in the helicity basis of the Z boson in the $q\bar{q}$ c.m. frame, and at the last equality the following 3×3 matrix form is employed:

$$\rho_{\sigma}(q\bar{q}) = \begin{pmatrix} \rho_{\sigma}^{++}(q\bar{q}) & \rho_{\sigma}^{+-}(q\bar{q}) & \rho_{\sigma}^{+0}(q\bar{q}) \\ \rho_{\sigma}^{-+}(q\bar{q}) & \rho_{\sigma}^{--}(q\bar{q}) & \rho_{\sigma}^{-0}(q\bar{q}) \\ \rho_{\sigma}^{0+}(q\bar{q}) & \rho_{\sigma}^{0-}(q\bar{q}) & \rho_{\sigma}^{00}(q\bar{q}) \end{pmatrix}, \quad d^{\tau} = \begin{pmatrix} d_{+}^{\tau} \\ d_{-}^{\tau} \\ d_{0}^{\tau} \end{pmatrix}.$$
(3.9)

The density matrix is a 3×3 Hermitian matrix: $\sum_{\sigma} \rho_{\sigma}(q\bar{q}) = (\sum_{\sigma} \rho_{\sigma}(q\bar{q}))^{\dagger}$ ⁵.

The full helicity amplitude $\mathcal{T}_{\sigma}^{\tau}(\bar{q}q)$, in which the production amplitude is evaluated in the $\bar{q}q$ c.m. frame shown in the right picture of Figure 3, can be treated in the same manner:

$$\mathcal{T}_{\sigma}^{\tau}(\bar{q}q) = P_Z \sum_{\lambda = \pm, 0} \mathcal{M}_{\sigma}^{\lambda}(\bar{q}q) \ D_{\lambda}^{\tau}, \tag{3.10a}$$

$$\begin{split} \sum_{\sigma} \left| \mathcal{T}_{\sigma}^{\tau}(\bar{q}q) \right|^2 &= \left| P_Z m_Z g_{Zf\bar{f}}^{\tau} \right|^2 \sum_{\sigma} \sum_{\lambda',\lambda} \left(d_{\lambda'}^{\tau} \right)^* \rho_{\sigma}^{\lambda'\lambda}(\bar{q}q) d_{\lambda}^{\tau} \\ &= \left| P_Z m_Z g_{Zf\bar{f}}^{\tau} \right|^2 d^{\tau\dagger} \sum_{\sigma} \rho_{\sigma}(\bar{q}q) d^{\tau}, \end{split} \tag{3.10b}$$

where

$$\sum_{\sigma} \rho_{\sigma}^{\lambda'\lambda}(\bar{q}q) = \sum_{\sigma} \{\mathcal{M}_{\sigma}^{\lambda'}(\bar{q}q)\}^* \mathcal{M}_{\sigma}^{\lambda}(\bar{q}q)$$
(3.11)

represents the elements of the density matrix in the helicity basis of the Z boson in the $\bar{q}q$ c.m. frame. The production amplitude $\mathcal{M}^{\lambda}_{\sigma}(\bar{q}q)$ is given in eq. (2.7).

⁵In general a density matrix ρ has a normalisation condition $tr(\rho) = 1$; see e.g. refs. [56–59]. However, we employ the non-normalised form such as eq. (3.8) and call it a density matrix in this paper. The degrees of freedom of our density matrices is, therefore, not 8 but 9.

Label	Integration over y	Integration over $\cos \theta$
\mathcal{A}	$\int_{-y_{\rm cut}}^{y_{\rm cut}} dy$	$\int_{-(1-\epsilon)}^{1-\epsilon} d\cos\theta$
\mathcal{B}	$\biggl(\int_0^{y_{\rm cut}}-\int_{-y_{\rm cut}}^0\biggr)dy$	$\int_{-(1-\epsilon)}^{1-\epsilon} d\cos\theta$
\mathcal{C}		$\left(\int_0^{1-\epsilon} - \int_{-(1-\epsilon)}^0 d\cos\theta\right)$
\mathcal{D}	$\biggl(\int_0^{y_{\rm cut}}-\int_{-y_{\rm cut}}^0\biggr)dy$	$\left(\int_0^{1-\epsilon} - \int_{-(1-\epsilon)}^0 d\cos\theta\right)$

Table 1: The 4 different approaches labelled \mathcal{A} , \mathcal{B} , \mathcal{C} and \mathcal{D} for performing integration over the rapidity y and the polar angle $\cos\theta$ in the differential cross section of eq. (3.12). A value of $y_{\rm cut}$ is $\ln\sqrt{s/\hat{s}}$; see eq. (3.14). A smaller value can be also chosen for $y_{\rm cut}$. A value of ϵ (0 $\leq \epsilon$ < 1) will be determined according to experimental conditions.

3.2 Decay angular distributions of the polarised Z boson

In terms of the density matrices defined in eqs. (3.8) and (3.11), the complete differential cross section for the process $pp \to ZH$ followed by $Z \to f\bar{f}$ in the narrow width approximation can be expressed as follows:

$$\begin{split} \frac{d\sigma}{d\hat{s}\;dy\;d\cos\theta\;d\cos\hat{\theta}\;d\hat{\phi}} = & \frac{m_Z k}{12288\pi^3\Gamma_Z s\hat{s}^{\frac{3}{2}}} \sum_f \sum_\tau \left|g_{Zf\bar{f}}^\tau\right|^2 C_f \\ & \times \sum_q \left[q(x_1)\bar{q}(x_2)\;d^{\tau\dagger}\sum_\sigma \rho_\sigma(q\bar{q})d^\tau + \bar{q}(x_1)q(x_2)\;d^{\tau\dagger}\sum_\sigma \rho_\sigma(\bar{q}q)d^\tau\right], \end{split} \tag{3.12}$$

where s is the c.m. energy squared of the pp collisions, \hat{s} is the c.m. energy squared of the $q\bar{q}$ collisions, y is the rapidity of the $q\bar{q}$ c.m. frame and the $\bar{q}q$ c.m. frame (see Figure 3) on the pp c.m. frame (i.e. the experimental frame), C_f is an effective colour factor: $C_f=1$ for Z decays into a charged lepton pair and $C_f=3$ for Z decays into a quark pair, $q(x_i)$ and $\bar{q}(x_i)$ are the quark and antiquark parton distribution functions (PDFs) with energy fraction x_i . Summations are performed over the final fermion flavor f, the helicity τ of the final fermion, and the initial quark and antiquark flavor f. Averages are performed over the helicity and colour of the initial quark, and those of the initial antiquark. Recall that f is the momentum of the f boson and f is the polar angle of the f boson in the f c.m. frame and the f c.m. frame. The decay angles f and f are defined in eq. (3.4). Here f c.m. frame and the f c.m. frame and f c.m. fram

$$\hat{s} = sx_1x_2, \quad y = \frac{1}{2}\ln\frac{x_1}{x_2}.$$
 (3.13)

The allowed region is

$$(m_Z + m_H)^2 < \hat{s} < s, -\ln\sqrt{\frac{s}{\hat{s}}} < y < \ln\sqrt{\frac{s}{\hat{s}}}.$$
 (3.14)

Now we derive the differential cross sections with respect to \hat{s} , $\cos \hat{\theta}$ and $\hat{\phi}$ by integrating over y and $\cos \theta$ in eq. (3.12). We consider the 4 different integration approaches summarised in Table 1. In the complete differential cross section of eq. (3.12), the polar angle θ dependence appears only

$$\begin{array}{cccc} c_1 & \frac{4}{3} - 2\epsilon + \epsilon^2 - \frac{1}{3}\epsilon^3 & \frac{4}{3} \\ c_2 & \frac{4}{3} - 2\epsilon^2 + \frac{2}{3}\epsilon^3 & \frac{4}{3} \\ c_3 & \frac{1}{\sqrt{2}} \left[(1 - \epsilon)\sqrt{\epsilon(2 - \epsilon)} + \sin^{-1}(1 - \epsilon) \right] & \frac{\pi}{2\sqrt{2}} \\ c_4 & \frac{2}{3\sqrt{2}} \left[1 - 2\epsilon\sqrt{\epsilon(2 - \epsilon)} + \sqrt{\epsilon^5(2 - \epsilon)} \right] & \frac{2}{3\sqrt{2}} \\ c_5 & 1 - 2\epsilon + \epsilon^2 & 1 \end{array}$$

Table 2: Constant coefficients in the density matrices after $\cos \theta$ integration; see eqs. (3.15) and (3.19). The last column gives the values for $\epsilon = 0$.

in $\rho_{\sigma}(q\bar{q})$ and $\rho_{\sigma}(\bar{q}q)$. The $\cos\theta$ integration in the approaches \mathcal{A} and \mathcal{B} results in

$$\langle \rho_{\sigma}(q\bar{q}) \rangle \equiv \int_{-(1-\epsilon)}^{1-\epsilon} d\cos\theta \ \rho_{\sigma}(q\bar{q}) = \begin{pmatrix} c_{1} |\hat{M}_{\sigma}^{+}|^{2} & \frac{1}{2}c_{2}(\hat{M}_{\sigma}^{+})^{*}\hat{M}_{\sigma}^{-} & c_{3}\sigma(\hat{M}_{\sigma}^{+})^{*}\hat{M}_{\sigma}^{0} \\ \frac{1}{2}c_{2}\hat{M}_{\sigma}^{+}(\hat{M}_{\sigma}^{-})^{*} & c_{1}|\hat{M}_{\sigma}^{-}|^{2} & c_{3}\sigma(\hat{M}_{\sigma}^{-})^{*}\hat{M}_{\sigma}^{0} \\ c_{3}\sigma\hat{M}_{\sigma}^{+}(\hat{M}_{\sigma}^{0})^{*} & c_{3}\sigma\hat{M}_{\sigma}^{-}(\hat{M}_{\sigma}^{0})^{*} & c_{2}|\hat{M}_{\sigma}^{0}|^{2} \end{pmatrix}$$
(3.15a)

and

$$\langle \rho_{\sigma}(\bar{q}q) \rangle \equiv \int_{-(1-\epsilon)}^{1-\epsilon} d\cos\theta \ \rho_{\sigma}(\bar{q}q) = \begin{pmatrix} c_1 |\hat{M}_{\sigma}^{+}|^2 & \frac{1}{2}c_2 (\hat{M}_{\sigma}^{+})^* \hat{M}_{\sigma}^{-} & -c_3 \sigma (\hat{M}_{\sigma}^{+})^* \hat{M}_{\sigma}^{0} \\ \frac{1}{2}c_2 \hat{M}_{\sigma}^{+} (\hat{M}_{\sigma}^{-})^* & c_1 |\hat{M}_{\sigma}^{-}|^2 & -c_3 \sigma (\hat{M}_{\sigma}^{-})^* \hat{M}_{\sigma}^{0} \\ -c_3 \sigma \hat{M}_{\sigma}^{+} (\hat{M}_{\sigma}^{0})^* & -c_3 \sigma \hat{M}_{\sigma}^{-} (\hat{M}_{\sigma}^{0})^* & c_2 |\hat{M}_{\sigma}^{0}|^2 \end{pmatrix},$$

$$(3.15b)$$

where c_i (i=1,2,3) are constant values depending on ϵ and summarised in Table 2, and $\hat{M}_{\sigma}^{\lambda=\pm,0}$ are defined in eq. (2.5). Notice the difference between eq. (3.15a) and eq. (3.15b) that there is a minus sign in front of the elements that have the overall σ in eq. (3.15b). This result is actually obvious from the comparison between the amplitudes in eq. (2.4) and those in eq. (2.7). After integration over y and $\cos \theta$ in the approach \mathcal{A} , the differential cross section can be expressed as

$$\begin{split} \frac{d\sigma}{d\hat{s}\;d\cos\hat{\theta}\;d\hat{\phi}}\bigg|_{\mathcal{A}} &= \mathcal{T}\int_{-y_{\text{cut}}}^{y_{\text{cut}}}dy\bigg[q(x_1)\bar{q}(x_2)\;d^{\tau\dagger}\sum_{\sigma}\langle\rho_{\sigma}(q\bar{q})\rangle d^{\tau} + \bar{q}(x_1)q(x_2)\;d^{\tau\dagger}\sum_{\sigma}\langle\rho_{\sigma}(\bar{q}q)\rangle d^{\tau}\bigg] \\ &= \mathcal{T}\int_{0}^{y_{\text{cut}}}dy\bigg[\underline{q(x_1)\bar{q}(x_2)}\;d^{\tau\dagger}\sum_{\sigma}\langle\rho_{\sigma}(q\bar{q})\rangle d^{\tau} + \underline{\bar{q}(x_1)q(x_2)}\;d^{\tau\dagger}\sum_{\sigma}\langle\rho_{\sigma}(\bar{q}q)\rangle d^{\tau}\bigg] \\ &+ \mathcal{T}\int_{-y_{\text{cut}}}^{0}dy\bigg[\underline{\bar{q}(x_2)q(x_1)}\;d^{\tau\dagger}\sum_{\sigma}\langle\rho_{\sigma}(q\bar{q})\rangle d^{\tau} + \underline{q(x_2)\bar{q}(x_1)}\;d^{\tau\dagger}\sum_{\sigma}\langle\rho_{\sigma}(\bar{q}q)\rangle d^{\tau}\bigg] \\ &= \mathcal{T}\int_{0}^{y_{\text{cut}}}dy\;2\Big[q(x_1)\bar{q}(x_2) + \bar{q}(x_1)q(x_2)\Big]d^{\tau\dagger}\sum_{\sigma}\begin{pmatrix}c_1|\hat{M}_{\sigma}^{+}|^2 & \frac{1}{2}c_2(\hat{M}_{\sigma}^{+})^*\hat{M}_{\sigma}^{-} & 0\\ \frac{1}{2}c_2\hat{M}_{\sigma}^{+}(\hat{M}_{\sigma}^{-})^* & c_1|\hat{M}_{\sigma}^{-}|^2 & 0\\ 0 & 0 & c_2|\hat{M}_{\sigma}^{0}|^2\end{pmatrix}d^{\tau}, \end{split}$$

where

$$\mathcal{T} = \frac{m_Z k}{12288\pi^3 \Gamma_Z s \hat{s}^{\frac{3}{2}}} \sum_f \sum_{\tau} |g_{Zf\bar{f}}^{\tau}|^2 C_f \sum_q$$
 (3.17)

is introduced to simplify our writing. The PDFs labelled A in the second equality (i.e. $q(x_1)\bar{q}(x_2)$ and $q(x_2)\bar{q}(x_1)$) give the same numerical contribution after integration over y, therefore they are combined in the third (i.e. last) equality. The same is done for the PDFs labelled B. In the last equality, $\langle \rho_{\sigma}(q\bar{q}) \rangle$ and $\langle \rho_{\sigma}(\bar{q}q) \rangle$ are added, and the elements that have the overall σ vanish due to the sign difference in $\langle \rho_{\sigma}(q\bar{q}) \rangle$ and $\langle \rho_{\sigma}(\bar{q}q) \rangle$. The vanished elements in the approach \mathcal{A} in

eq. (3.16) revive by performing integration in the approach \mathcal{B} :

$$\frac{d\sigma}{d\hat{s} \ d\cos\hat{\theta} \ d\hat{\phi}}\Big|_{\mathcal{B}} = \mathcal{T}\left(\int_{0}^{y_{\text{cut}}} - \int_{-y_{\text{cut}}}^{0} dy \left[q(x_{1})\bar{q}(x_{2}) \ d^{\tau\dagger} \sum_{\sigma} \left\langle \rho_{\sigma}(q\bar{q}) \right\rangle d^{\tau} + \bar{q}(x_{1})q(x_{2}) \ d^{\tau\dagger} \sum_{\sigma} \left\langle \rho_{\sigma}(\bar{q}q) \right\rangle d^{\tau} \right] \\
= \mathcal{T}\int_{0}^{y_{\text{cut}}} dy \left[\underbrace{q(x_{1})\bar{q}(x_{2})}_{A} \ d^{\tau\dagger} \sum_{\sigma} \left\langle \rho_{\sigma}(q\bar{q}) \right\rangle d^{\tau} + \underbrace{\bar{q}(x_{1})q(x_{2})}_{B} \ d^{\tau\dagger} \sum_{\sigma} \left\langle \rho_{\sigma}(\bar{q}q) \right\rangle d^{\tau} \right] \\
- \mathcal{T}\int_{0}^{y_{\text{cut}}} dy \left[\underbrace{\bar{q}(x_{2})q(x_{1})}_{B} \ d^{\tau\dagger} \sum_{\sigma} \left\langle \rho_{\sigma}(q\bar{q}) \right\rangle d^{\tau} + \underbrace{q(x_{2})\bar{q}(x_{1})}_{A} \ d^{\tau\dagger} \sum_{\sigma} \left\langle \rho_{\sigma}(\bar{q}q) \right\rangle d^{\tau} \right] \\
= \mathcal{T}\int_{0}^{y_{\text{cut}}} dy \ 2\left[q(x_{1})\bar{q}(x_{2}) - \bar{q}(x_{1})q(x_{2})\right] d^{\tau\dagger} \sum_{\sigma} \left(\begin{array}{ccc} 0 & 0 & c_{3}\sigma(\hat{M}_{\sigma}^{+})^{*}\hat{M}_{\sigma}^{0} \\ c_{3}\sigma\hat{M}_{\sigma}^{+}(\hat{M}_{\sigma}^{0})^{*} & c_{3}\sigma\hat{M}_{\sigma}^{-}(\hat{M}_{\sigma}^{0})^{*} & 0 \\ (3.18) & (3.18) \end{array}\right) d^{\tau},$$

where, in the last equality, $\langle \rho_{\sigma}(q\bar{q}) \rangle$ and $\langle \rho_{\sigma}(\bar{q}q) \rangle$ are subtracted. As a result, in contrast to the approach \mathcal{A} , only the elements that have the overall σ survive.

The $\cos \theta$ integration in the approaches \mathcal{C} and \mathcal{D} results in

$$\overline{\left< \rho_{\sigma}(q\bar{q}) \right>} \equiv \left(\int_{0}^{1-\epsilon} - \int_{-(1-\epsilon)}^{0} \right) d\cos\theta \ \rho_{\sigma}(q\bar{q}) = \left(\begin{array}{ccc} c_{5}\sigma \left| \hat{M}_{\sigma}^{+} \right|^{2} & 0 & c_{4} \left(\hat{M}_{\sigma}^{+} \right)^{*} \hat{M}_{\sigma}^{0} \\ 0 & -c_{5}\sigma \left| \hat{M}_{\sigma}^{-} \right|^{2} & -c_{4} \left(\hat{M}_{\sigma}^{-} \right)^{*} \hat{M}_{\sigma}^{0} \\ c_{4} \hat{M}_{\sigma}^{+} \left(\hat{M}_{\sigma}^{0} \right)^{*} & -c_{4} \hat{M}_{\sigma}^{-} \left(\hat{M}_{\sigma}^{0} \right)^{*} & 0 \end{array} \right)$$

$$(3.19a)$$

and

$$\overline{\langle \rho_{\sigma}(\bar{q}q) \rangle} \equiv \left(\int_{0}^{1-\epsilon} - \int_{-(1-\epsilon)}^{0} \right) d\cos\theta \ \rho_{\sigma}(\bar{q}q) = \begin{pmatrix} -c_{5}\sigma |\hat{M}_{\sigma}^{+}|^{2} & 0 & c_{4}(\hat{M}_{\sigma}^{+})^{*}\hat{M}_{\sigma}^{0} \\ 0 & c_{5}\sigma |\hat{M}_{\sigma}^{-}|^{2} & -c_{4}(\hat{M}_{\sigma}^{-})^{*}\hat{M}_{\sigma}^{0} \\ c_{4}\hat{M}_{\sigma}^{+}(\hat{M}_{\sigma}^{0})^{*} & -c_{4}\hat{M}_{\sigma}^{-}(\hat{M}_{\sigma}^{0})^{*} & 0 \end{pmatrix}, \tag{3.19b}$$

where the constant values c_i (i=4,5) are summarised in Table 2. Notice again that the sign in front of the elements that have the overall σ is different between $\overline{\langle \rho_{\sigma}(q\bar{q}) \rangle}$ and $\overline{\langle \rho_{\sigma}(\bar{q}q) \rangle}$. The integration over y and $\cos\theta$ in the approaches $\mathcal C$ and $\mathcal D$ proceeds in the same manners as eq. (3.16) and eq. (3.18), respectively:

$$\begin{split} \frac{d\sigma}{d\hat{s}\;d\cos\hat{\theta}\;d\hat{\phi}}\bigg|_{\mathcal{C}} &= \mathcal{T} \int_{-y_{\mathrm{cut}}}^{y_{\mathrm{cut}}} dy \bigg[q(x_1)\bar{q}(x_2)\;d^{\tau\dagger} \sum_{\sigma} \overline{\left\langle \rho_{\sigma}(q\bar{q})\right\rangle} d^{\tau} + \bar{q}(x_1)q(x_2)\;d^{\tau\dagger} \sum_{\sigma} \overline{\left\langle \rho_{\sigma}(\bar{q}q)\right\rangle} d^{\tau}\bigg] \\ &= \mathcal{T} \int_{0}^{y_{\mathrm{cut}}} dy\; 2 \Big[q(x_1)\bar{q}(x_2) + \bar{q}(x_1)q(x_2)\Big] d^{\tau\dagger} \sum_{\sigma} \left(\begin{array}{ccc} 0 & 0 & c_4 \left(\hat{M}_{\sigma}^+\right)^* \hat{M}_{\sigma}^0 \\ 0 & 0 & -c_4 \left(\hat{M}_{\sigma}^-\right)^* \hat{M}_{\sigma}^0 \\ c_4 \hat{M}_{\sigma}^+ \left(\hat{M}_{\sigma}^0\right)^* & -c_4 \hat{M}_{\sigma}^- \left(\hat{M}_{\sigma}^0\right)^* & 0 \\ \end{array} \right) d^{\tau}, \end{split}$$

$$\frac{d\sigma}{d\hat{s} \ d\cos\hat{\theta} \ d\hat{\phi}} \Big|_{\mathcal{D}} = \mathcal{T} \left(\int_{0}^{y_{\text{cut}}} - \int_{-y_{\text{cut}}}^{0} \right) dy \left[q(x_{1})\bar{q}(x_{2}) \ d^{\tau\dagger} \sum_{\sigma} \overline{\langle \rho_{\sigma}(q\bar{q}) \rangle} d^{\tau} + \bar{q}(x_{1})q(x_{2}) \ d^{\tau\dagger} \sum_{\sigma} \overline{\langle \rho_{\sigma}(\bar{q}q) \rangle} d^{\tau} \right] \\
= \mathcal{T} \int_{0}^{y_{\text{cut}}} dy \ 2 \left[q(x_{1})\bar{q}(x_{2}) - \bar{q}(x_{1})q(x_{2}) \right] d^{\tau\dagger} \sum_{\sigma} \begin{pmatrix} c_{5}\sigma |\hat{M}_{\sigma}^{+}|^{2} & 0 & 0 \\ 0 & -c_{5}\sigma |\hat{M}_{\sigma}^{-}|^{2} & 0 \\ 0 & 0 & 0 \end{pmatrix} d^{\tau}. \tag{3.21}$$

Only the elements that do not have the overall σ survive in eq. (3.20), while only the elements that have the overall σ survive in eq. (3.21).

The differential cross sections with respect to \hat{s} and the decay angles $\hat{\theta}$ and $\hat{\phi}$ have 9 independent angular distributions and can be expressed as

$$\frac{d\sigma}{d\hat{s} \, d\cos\hat{\theta} \, d\hat{\phi}}\Big|_{i(=\mathcal{A},\mathcal{B},\mathcal{C},\mathcal{D})} = F_{i1} \left(1 + \cos^2\hat{\theta}\right) + F_{i2} \left(1 - 3\cos^2\hat{\theta}\right) + F_{i3}\cos\hat{\theta}
+ F_{i4}\sin\hat{\theta}\cos\hat{\phi} + F_{i5}\sin2\hat{\theta}\cos\hat{\phi} + F_{i6}\sin^2\hat{\theta}\cos2\hat{\phi}
+ F_{i7}\sin\hat{\theta}\sin\hat{\phi} + F_{i8}\sin2\hat{\theta}\sin\hat{\phi} + F_{i9}\sin^2\hat{\theta}\sin2\hat{\phi},$$
(3.22)

where the coefficients F_{ia} $(i = \mathcal{A}, \mathcal{B}, \mathcal{C}, \mathcal{D})$ $(a = 1, 2, \dots, 9)$ are functions of \hat{s} and written in terms of the non-vanishing elements in eqs. (3.16), (3.18), (3.20) and (3.21). Note that there are in total $36 \ (= 4 \times 9)$ coefficients. It is straightforward to obtain the explicit form of the coefficients F_{ia} $(i = \mathcal{A}, \mathcal{B}, \mathcal{C}, \mathcal{D})$ $(a = 1, 2, \dots, 9)$:

$$F_{\mathcal{A}(\mathcal{C})a} = \mathcal{T} \int_{0}^{y_{\text{cut}}} dy \ 2 \Big[q(x_1)\bar{q}(x_2) + \bar{q}(x_1)q(x_2) \Big] \sum_{\sigma} f_{\mathcal{A}(\mathcal{C})a}, \tag{3.23a}$$

$$F_{\mathcal{B}(\mathcal{D})a} = \mathcal{T} \int_0^{y_{\text{cut}}} dy \ 2 \Big[q(x_1) \bar{q}(x_2) - \bar{q}(x_1) q(x_2) \Big] \sum_{\sigma} f_{\mathcal{B}(\mathcal{D})a},$$
 (3.23b)

where

$$f_{\mathcal{A}1} = \frac{1}{2} (c_1 |\hat{M}_{\sigma}^+|^2 + c_1 |\hat{M}_{\sigma}^-|^2 + c_2 |\hat{M}_{\sigma}^0|^2), \qquad f_{\mathcal{B}1} = 0,$$

$$f_{\mathcal{A}2} = \frac{1}{2} c_2 |\hat{M}_{\sigma}^0|^2, \qquad f_{\mathcal{B}2} = 0,$$

$$f_{\mathcal{A}3} = c_1 (|\hat{M}_{\sigma}^+|^2 - |\hat{M}_{\sigma}^-|^2)\tau, \qquad f_{\mathcal{B}3} = 0,$$

$$f_{\mathcal{A}4} = 0, \qquad f_{\mathcal{B}4} = \sqrt{2}\sigma c_3 Re \left[(\hat{M}_{\sigma}^+)^* \hat{M}_{\sigma}^0 + (\hat{M}_{\sigma}^0)^* \hat{M}_{\sigma}^- \right]\tau,$$

$$f_{\mathcal{A}5} = 0, \qquad f_{\mathcal{B}5} = \frac{1}{\sqrt{2}} \sigma c_3 Re \left[(\hat{M}_{\sigma}^+)^* \hat{M}_{\sigma}^0 - (\hat{M}_{\sigma}^0)^* \hat{M}_{\sigma}^- \right],$$

$$f_{\mathcal{A}6} = \frac{1}{2} c_2 Re \left[(\hat{M}_{\sigma}^+)^* \hat{M}_{\sigma}^0 \right], \qquad f_{\mathcal{B}6} = 0,$$

$$f_{\mathcal{A}7} = 0, \qquad f_{\mathcal{B}7} = \sqrt{2}\sigma c_3 Im \left[(\hat{M}_{\sigma}^+)^* \hat{M}_{\sigma}^0 + (\hat{M}_{\sigma}^0)^* \hat{M}_{\sigma}^- \right]\tau,$$

$$f_{\mathcal{A}8} = 0, \qquad f_{\mathcal{B}8} = \frac{1}{\sqrt{2}} \sigma c_3 Im \left[(\hat{M}_{\sigma}^+)^* \hat{M}_{\sigma}^0 - (\hat{M}_{\sigma}^0)^* \hat{M}_{\sigma}^- \right],$$

$$f_{\mathcal{A}9} = \frac{1}{2} c_2 Im \left[(\hat{M}_{\sigma}^+)^* \hat{M}_{\sigma}^0 \right], \qquad f_{\mathcal{B}9} = 0, \qquad (3.24a)$$

and

$$f_{C1} = 0, f_{D1} = \frac{1}{2}\sigma c_{5}(|\hat{M}_{\sigma}^{+}|^{2} - |\hat{M}_{\sigma}^{-}|^{2}),$$

$$f_{C2} = 0, f_{D3} = 0, f_{D3} = \sigma c_{5}(|\hat{M}_{\sigma}^{+}|^{2} + |\hat{M}_{\sigma}^{-}|^{2})\tau,$$

$$f_{C4} = \sqrt{2}c_{4}Re[(\hat{M}_{\sigma}^{+})^{*}\hat{M}_{\sigma}^{0} - (\hat{M}_{\sigma}^{0})^{*}\hat{M}_{\sigma}^{-}]\tau, f_{D4} = 0,$$

$$f_{C5} = \frac{1}{\sqrt{2}}c_{4}Re[(\hat{M}_{\sigma}^{+})^{*}\hat{M}_{\sigma}^{0} + (\hat{M}_{\sigma}^{0})^{*}\hat{M}_{\sigma}^{-}], f_{D5} = 0,$$

$$f_{C6} = 0, f_{D6} = 0,$$

$$f_{C7} = \sqrt{2}c_{4}Im[(\hat{M}_{\sigma}^{+})^{*}\hat{M}_{\sigma}^{0} - (\hat{M}_{\sigma}^{0})^{*}\hat{M}_{\sigma}^{-}]\tau, f_{D7} = 0,$$

$$f_{C8} = \frac{1}{\sqrt{2}}c_{4}Im[(\hat{M}_{\sigma}^{+})^{*}\hat{M}_{\sigma}^{0} + (\hat{M}_{\sigma}^{0})^{*}\hat{M}_{\sigma}^{-}], f_{D8} = 0,$$

$$f_{D9} = 0, f_{D9} = 0. (3.24b)$$

Among the 36 coefficients, only the 15 coefficients can be non-zero. It is easy to notice that there are the 10 combinations of the elements of the density matrix in total. However, only 9 of them are independent ⁶. Some of them are strictly zero, if the amplitudes satisfy the restriction in eq. (2.13a)

⁶Among the 3 combinations in f_{A1} , f_{A2} and f_{D3} , only 2 of them are independent, since one of them can be constructed from the other two.

from CP invariance and/or the restriction in eq. (2.15a) from CPT invariance. For example, by applying the restrictions in eqs. (2.13a) and (2.15a) to the combination in $f_{\mathcal{A}9}$, we find

$$CP \text{ invariance}: Im\left[\left(\hat{M}_{\sigma}^{+}\right)^{*}\hat{M}_{\sigma}^{-}\right] = Im\left[\left|\hat{M}_{\sigma}^{+}\right|^{2}\right] = 0,$$

$$CP\widetilde{T} \text{ invariance}: Im\left[\left(\hat{M}_{\sigma}^{+}\right)^{*}\hat{M}_{\sigma}^{-}\right] = Im\left[\left(\hat{M}_{\sigma}^{-}\right)^{2}\right] \neq 0,$$

$$(3.25)$$

where the former means that CP invariance requires it to be zero, while the latter means that $CP\widetilde{T}$ invariance does not require it to be zero. This indicates that observation of a nonzero value in $F_{\mathcal{A}9}$ signals CP violation. Similarly, by applying the restrictions in eqs. (2.13a) and (2.15a) to the combination in $f_{\mathcal{B}8}$ and $f_{\mathcal{C}7}$, we find

$$CP \text{ invariance}: Im \left[(\hat{M}_{\sigma}^{+})^{*} \hat{M}_{\sigma}^{0} - (\hat{M}_{\sigma}^{0})^{*} \hat{M}_{\sigma}^{-} \right] = Im \left[(\hat{M}_{\sigma}^{+})^{*} \hat{M}_{\sigma}^{0} - \left\{ (\hat{M}_{\sigma}^{+})^{*} \hat{M}_{\sigma}^{0} \right\}^{*} \right] \neq 0,$$

$$CP\widetilde{T} \text{ invariance}: Im \left[(\hat{M}_{\sigma}^{+})^{*} \hat{M}_{\sigma}^{0} - (\hat{M}_{\sigma}^{0})^{*} \hat{M}_{\sigma}^{-} \right] = Im \left[(\hat{M}_{\sigma}^{+})^{*} \hat{M}_{\sigma}^{0} - \hat{M}_{\sigma}^{0} (\hat{M}_{\sigma}^{+})^{*} \right] = 0, \quad (3.26)$$

where $CP\widetilde{T}$ invariance requires it to be zero, while CP invariance does not. This indicates that observation of a nonzero value in $F_{\mathcal{B}8}$ or $F_{\mathcal{C}7}$ signals $CP\widetilde{T}$ violation. The symmetry properties of the 10 combinations are summarised in Table 3. The symbol + means that the symmetry does not require the combination to be zero, while - means that the symmetry requires the combination to be zero. We also show the coefficients F_{ia} by measuring which the combinations of the density matrix elements can be determined. The symbol \circ in the column "f charge" means that observation of the coefficient F_{ia} requires distinguishing the fermion f from the antifermion \bar{f} . In other words, it requires identification of the charge (flavor) of the final fermion f. This can be confirmed by performing a translation $\hat{\theta} \to \pi - \hat{\theta}$ and $\hat{\phi} \to \hat{\phi} + \pi$ in eq. (3.22) and observing the change of the sign. Among the 15 coefficients, only 9 of them do not require the charge identification of the final fermion f. It should be emphasised that these 9 coefficients are necessary and sufficient to determine all of the 9 independent combinations of the density matrix elements.

The coefficients F_{ia} ($i = \mathcal{A}, \mathcal{B}, \mathcal{C}, \mathcal{D}$) ($a = 1, 2, \dots, 9$) will be experimentally determined by measuring the decay angles $\widehat{\theta}$ and $\widehat{\phi}$ in the rest frame of the Z boson (see eq. (3.4)), since we completely know the differential angular distributions as eq. (3.22). We just do not know the coefficients F_{ia} which uniquely depend on a state of polarisation of the Z boson. With appropriate integration over $\cos \widehat{\theta}$ and $\widehat{\phi}$, it is possible to isolate the angular distributions:

$$\int_{-1}^{1} d\cos\widehat{\theta} \frac{d\sigma}{d\widehat{s}d\cos\widehat{\theta}d\widehat{\phi}} = \frac{8}{3}F_{1} + \frac{\pi}{2}F_{4}\cos\widehat{\phi} + \frac{4}{3}F_{6}\cos2\widehat{\phi} + \frac{\pi}{2}F_{7}\sin\widehat{\phi} + \frac{4}{3}F_{9}\sin2\widehat{\phi}, \tag{3.27a}$$

$$\left(\int_{0}^{1} - \int_{-1}^{0} d\cos \widehat{\theta} \frac{d\sigma}{d\widehat{s}d\cos \widehat{\theta}d\widehat{\phi}} = F_{3} + \frac{4}{3}F_{5}\cos \widehat{\phi} + \frac{4}{3}F_{8}\sin \widehat{\phi},$$
(3.27b)

and

$$\frac{1}{2\pi} \int_0^{2\pi} d\widehat{\phi} \frac{d\sigma}{d\widehat{s}d\cos\widehat{\theta}d\widehat{\phi}} = F_1 \left(1 + \cos^2\widehat{\theta} \right) + F_2 \left(1 - 3\cos^2\widehat{\theta} \right) + F_3 \cos\widehat{\theta},$$
(3.28a)

$$\frac{1}{4} \left(\int_0^{\pi/2} - \int_{\pi/2}^{\pi} - \int_{\pi}^{3\pi/2} + \int_{3\pi/2}^{2\pi} \right) d\widehat{\phi} \frac{d\sigma}{d\widehat{s}d\cos\widehat{\theta}d\widehat{\phi}} = F_4 \sin\widehat{\theta} + F_5 \sin 2\widehat{\theta}, \tag{3.28b}$$

$$\frac{1}{4} \left(\int_0^{\pi/4} - \int_{\pi/4}^{\pi/2} - \int_{\pi/2}^{3\pi/4} + \int_{3\pi/4}^{\pi} + \int_{\pi}^{5\pi/4} - \int_{5\pi/4}^{3\pi/2} - \int_{3\pi/2}^{7\pi/4} + \int_{7\pi/4}^{2\pi} \right) d\widehat{\phi} \frac{d\sigma}{d\widehat{s}d\cos\widehat{\theta}d\widehat{\phi}} = F_6 \sin^2\widehat{\theta}, \tag{3.28c}$$

$$\frac{1}{4} \left(\int_0^{\pi} - \int_{\pi}^{2\pi} d\hat{\phi} \frac{d\sigma}{d\hat{s}d\cos\hat{\theta}d\hat{\phi}} = F_7 \sin\hat{\theta} + F_8 \sin 2\hat{\theta},$$
 (3.28d)

$$\frac{1}{4} \left(\int_0^{\pi/2} - \int_{\pi/2}^{\pi} + \int_{\pi}^{3\pi/2} - \int_{3\pi/2}^{2\pi} \right) d\widehat{\phi} \frac{d\sigma}{d\widehat{s}d\cos\widehat{\theta}d\widehat{\phi}} = F_9 \sin^2\widehat{\theta}. \tag{3.28e}$$

Here the index i = A, B, C, D is omitted. By combining the 2 approaches in eq. (3.27) and the 5 approaches in eq. (3.28), we obtain the 10 (= 2 × 5) combinations. The 2 of them simply give zero (i.e. eqs. (3.27b) and (3.28c), and eqs. (3.27b) and (3.28e)). Each of the remaining 8 combinations gives one of F_a (a = 1, 3, 4, 5, 6, 7, 8, 9). For example, eqs. (3.27b) and (3.28b) gives F_5 . Only F_2 is not determined in this method. By a fitting procedure in the differential cross section with respect to \hat{s} and $\cos \hat{\theta}$ in eq. (3.28a), F_2 may be determined.

Combinations of	Symmetry properties		Observables	f charge	$HZ\gamma$	d.o.p
the density matrix elements	\overline{CP}	$CP\widetilde{T}$	•			
$\frac{1}{c_1 \hat{M}_{\sigma}^+ ^2 + c_1 \hat{M}_{\sigma}^- ^2 + c_2 \hat{M}_{\sigma}^0 ^2}$	+	+	F_{A1}	-	-	_
$\left \hat{M}_{\sigma}^{0}\right ^{2}$	+	+	$F_{\mathcal{A}2}$	-	-	-
$\left \hat{M}_{\sigma}^{+}\right ^{2}+\left \hat{M}_{\sigma}^{-}\right ^{2}$	+	+	$F_{\mathcal{D}3}$	0	0	0
$\left \hat{M}_{\sigma}^{+}\right ^{2}-\left \hat{M}_{\sigma}^{-}\right ^{2}$	_	_	$F_{\mathcal{A}3}$	0	-	-
F (^)) \ ^			$F_{\mathcal{D}1}$	-	0	0
$Re\left[\left(\hat{M}_{\sigma}^{+}\right)^{*}\hat{M}_{\sigma}^{0}+\left(\hat{M}_{\sigma}^{0}\right)^{*}\hat{M}_{\sigma}^{-}\right]$	+	+	$F_{\mathcal{B}4}$	0	0	0
[/_^\ * -^-0			F_{C5}	-	-	-
$Re\left[\left(\hat{M}_{\sigma}^{+}\right)^{*}\hat{M}_{\sigma}^{0}-\left(\hat{M}_{\sigma}^{0}\right)^{*}\hat{M}_{\sigma}^{-}\right]$	_	_	$F_{\mathcal{B}5}$	-	0	0
D [(a^r_)*a^r_]			$F_{\mathcal{C}4}$	0	-	-
$Re\left[\left(\hat{M}_{\sigma}^{+}\right)^{*}\hat{M}_{\sigma}^{-}\right]$	+	+	$F_{\mathcal{A}6}$	-	-	-
$Im\left[\left(\hat{M}_{\sigma}^{+}\right)^{*}\hat{M}_{\sigma}^{0}+\left(\hat{M}_{\sigma}^{0}\right)^{*}\hat{M}_{\sigma}^{-}\right]$	_	+	$F_{\mathcal{B}7}$	0	0	0
			$F_{\mathcal{C}8}$	-	-	-
$Im\left[\left(\hat{M}_{\sigma}^{+}\right)^{*}\hat{M}_{\sigma}^{0}-\left(\hat{M}_{\sigma}^{0}\right)^{*}\hat{M}_{\sigma}^{-}\right]$	+	_	$F_{\mathcal{B}8}$	-	0	0
			$F_{\mathcal{C}7}$	0	-	-
$Im\left[\left(\hat{M}_{\sigma}^{+}\right)^{*}\hat{M}_{\sigma}^{-}\right]$	_	+	$F_{\mathcal{A}9}$	-	-	-

Table 3: Symmetry properties of the 10 combinations of the density matrix elements. The coefficients F_{ia} of the differential angular distributions, by measuring which the combinations of the density matrix elements can be determined, are also shown. The symbol – means that the symmetry (CP or $CP\tilde{T}$) requires the combination to be zero, while the symbol + means that the symmetry does not; observation of a non-zero value in the combination with the symbol – under CP, for instance, signals CP violation. The symbol \circ in the column "f charge" means that observation of the coefficient F_{ia} requires the charge (or flavor) identification of the final fermion f. The symbol \circ in the column " $HZ\gamma$ " indicates that the coefficient F_{ia} has a good sensitivity to the $HZ\gamma$ coupling; see a discussion at the paragraph of eq. (3.29). The symbol \circ in the last column indicates that the coefficient F_{ia} is weakened according to the degree of polarisation of the Z boson; see a discussion at the last paragraph of Section 4.3. By the simple replacements $\hat{M}_{\sigma}^{\lambda} \to \hat{N}^{\lambda}$ and $F_{ia} \to F_{ia}^{W}$, the table corresponding to the process $pp \to W^{\pm}H$ is immediately obtained; see Section 4.

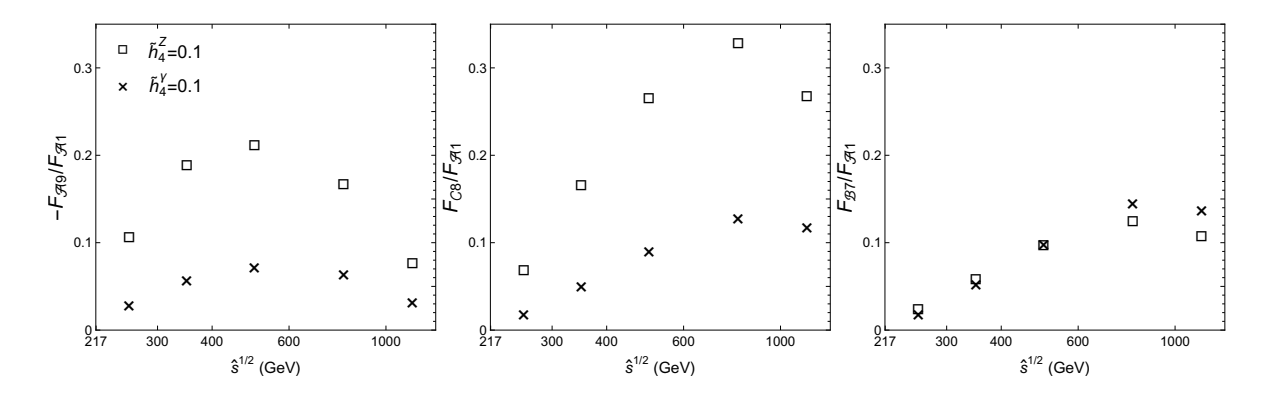


Figure 5: The coefficients $-F_{\mathcal{A}9}$ (left panel), $F_{\mathcal{C}8}$ (middle panel) and $F_{\mathcal{B}7}$ (right panel) divided by $F_{\mathcal{A}1}$ are shown. These coefficients are constrained to be identically zero by CP invariance. In each panel, \square points give predictions for $\widetilde{h}_4^Z=0.1$, and \times points give those for $\widetilde{h}_4^\gamma=0.1$. For each result, the values in the 5 bins, from left to right, are obtained after integration over \hat{s} in the regions $(m_Z+m_H)<\hat{s}^{1/2}<300$, $300<\hat{s}^{1/2}<400$, $400<\hat{s}^{1/2}<600$, $600<\hat{s}^{1/2}<1000$ and $1000<\hat{s}^{1/2}<14000$ in units of GeV.

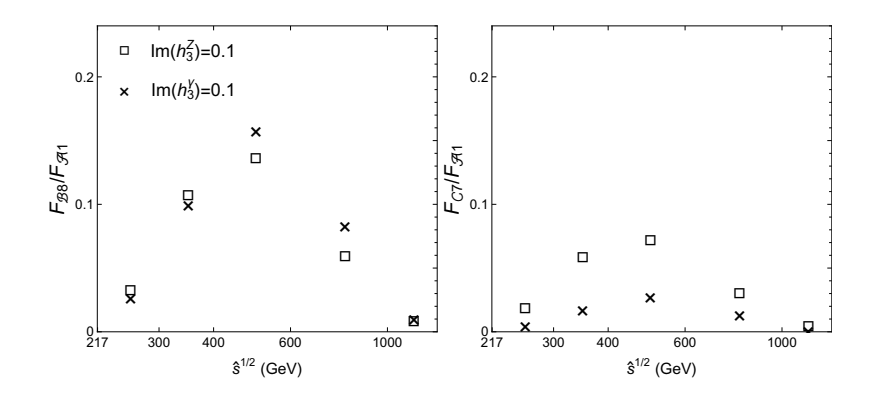


Figure 6: The coefficients $F_{\mathcal{B}8}$ (left panel) and $F_{\mathcal{C}7}$ (right panel) divided by $F_{\mathcal{A}1}$ are shown in the same manner as Figure 5. These coefficients are constrained to be identically zero by $CP\widetilde{T}$ invariance. In each panel, \square points give predictions for $h_3^Z = 0 + 0.1i$, and \times points give those for $h_3^{\gamma} = 0 + 0.1i$.

3.3 Influences of non-standard HZZ and $HZ\gamma$ interactions

In the previous section, we have clarified the restrictions on the coefficients of the differential angular distributions imposed by the CP and $CP\tilde{T}$ symmetries; see Table 3. Some of the coefficients are strictly zero in the SM due to CP invariance and some of them are small in the SM due to the smallness of re-scattering effects. These coefficients are in particular interesting as observables at the LHC, since observation of a non-zero or large value in these coefficients immediately signals the existence of physics beyond the SM. In this Section, we focus on these coefficients and study the influences of the non-standard HZZ and $HZ\gamma$ couplings.

Our numerical results are produced for the 14 TeV LHC. We set $m_H = 125.5$ GeV, and $\epsilon = 0$ in the $\cos\theta$ integration; see eqs. (3.15) and (3.19), and Table 2. As the final fermion flavor f summed in eq. (3.17), only the electron and the muon are considered when calculating the coefficients F_{ia} ($i = \mathcal{A}, \mathcal{B}, \mathcal{C}, \mathcal{D}$) (a = 3, 4, 7) (Recall that observation of these coefficients requires the charge identification of f), and all the quark flavors but the top quark are additionally considered when calculating the other coefficients. MSTW PDFs [70] are used. The phase space integration is performed with the program BASES [71].

In Figure 5, the coefficients $-F_{\mathcal{A}9}$ (left panel), $F_{\mathcal{C}8}$ (middle panel) and $F_{\mathcal{B}7}$ (right panel) divided by $F_{\mathcal{A}1}$ are shown 7 . For each result, the values in the 5 bins, from left to right, are obtained after integration over \hat{s} in the regions $(m_Z+m_H)<\hat{s}^{1/2}<300,\ 300<\hat{s}^{1/2}<400,\ 400<\hat{s}^{1/2}<600,\ 600<\hat{s}^{1/2}<1000$ and $1000<\hat{s}^{1/2}<14000$ in units of GeV. In each panel, \square points give predictions for the CP-odd form factor $\widetilde{h}_4^Z=0.1$, and \times points give those for the

When calculating F_{A1} , by which F_{ia} (i = A, B, C, D) (a = 3, 4, 7) are divided, we consider only the electron and the muon as the final fermion flavor f summed in eq. (3.17).

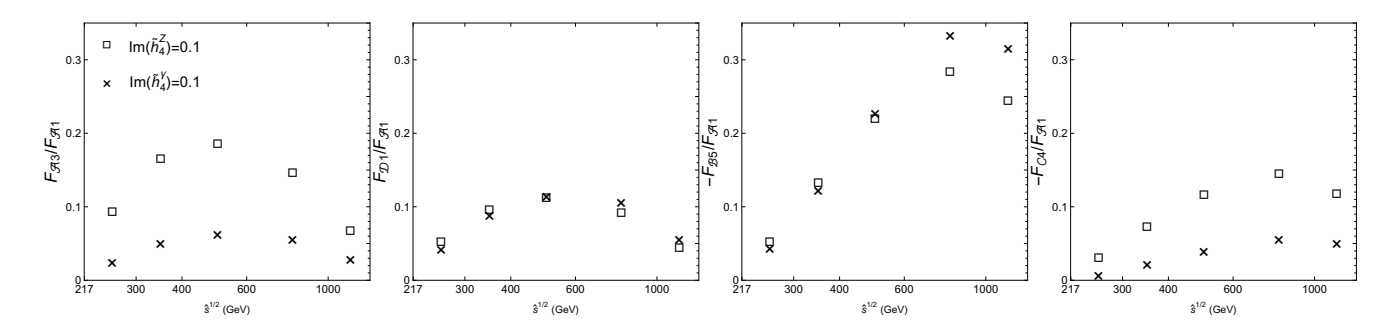


Figure 7: The angular coefficients $F_{\mathcal{A}3}$ (left panel), $F_{\mathcal{D}1}$ (middle-left panel), $-F_{\mathcal{B}5}$ (middle-right panel) and $-F_{\mathcal{C}4}$ (right panel) divided by $F_{\mathcal{A}1}$ are shown in the same manner as Figure 5. These coefficients are doubly constrained to be identically zero by CP invariance and $CP\tilde{T}$ invariance. In each panel, \square points give predictions for $\tilde{h}_4^Z = 0 + 0.1i$ and \times points give those for $\tilde{h}_4^Q = 0 + 0.1i$.

CP-odd form factor $\widetilde{h}_4^{\gamma}=0.1$. CP invariance requires these 4 coefficients to be identically zero, thus observation of a non-zero value signals CP violation.

The coefficients $F_{\mathcal{C}8}$ and $F_{\mathcal{B}7}$ measure the same combination of the density matrix elements (see Table 3), thus show the same dependence on $\hat{s}^{1/2}$. However, $F_{\mathcal{C}8}$'s sensitivity to \tilde{h}_4^Z is stronger than its sensitivity to \tilde{h}_4^{γ} , while $F_{\mathcal{B}7}$'s sensitivity to \tilde{h}_4^Z is comparable to its sensitivity to \tilde{h}_4^{γ} . This difference originates from the overall σ in $f_{\mathcal{B}7}$ and is explained as follows. Eq. (2.5) shows that \hat{M}_+^{λ} and \hat{M}_-^{λ} can be written in the following simplified form as the sum of the Z boson contribution and the γ contribution:

$$\hat{M}_{+}^{\lambda} = g_{Z+} f_{Z}^{\lambda} + f_{\gamma}^{\lambda}, \tag{3.29a}$$

$$\hat{M}_{-}^{\lambda} = g_{Z-} f_{Z}^{\lambda} + f_{\gamma}^{\lambda}. \tag{3.29b}$$

By using this expression, we derive

$$(\hat{M}_{+}^{\lambda'})^* \times \hat{M}_{+}^{\lambda} = g_{Z+}^2 (f_Z^{\lambda'})^* f_Z^{\lambda} + g_{Z+} [(f_Z^{\lambda'})^* f_{\gamma}^{\lambda} + (f_{\gamma}^{\lambda'})^* f_Z^{\lambda}] + (f_{\gamma}^{\lambda'})^* f_{\gamma}^{\lambda}, \tag{3.30a}$$

$$(\hat{M}_{-}^{\lambda'})^* \times \hat{M}_{-}^{\lambda} = g_{Z-}^2 (f_Z^{\lambda'})^* f_Z^{\lambda} + g_{Z-} [(f_Z^{\lambda'})^* f_{\gamma}^{\lambda} + (f_{\gamma}^{\lambda'})^* f_Z^{\lambda}] + (f_{\gamma}^{\lambda'})^* f_{\gamma}^{\lambda}. \tag{3.30b}$$

The couplings g_{Z+} and g_{Z-} have opposite signs to each other, both for the up-type quarks and for the down-type quarks. The interference term between the Z boson contribution and the γ contribution in eq. (3.30a) and that in eq. (3.30b), therefore, have opposite signs to each other, too. Considering $f_{\gamma}^{\lambda} = 0$ at the tree level approximation in the SM, the interference terms may give a larger contribution than the $(f_{\gamma}^{\lambda'})^* f_{\gamma}^{\lambda}$ term. The coefficient F_{C8} has a structure that eq. (3.30a) and eq. (3.30b) are added and the interference terms tend to cancel to each other. On the other hand, $F_{\mathcal{B}7}$ has a structure that eq. (3.30b) and eq. (3.30a) are subtracted due to the overall σ in $f_{\mathcal{B}7}$, and the interference terms contribute in the same direction. Therefore, as long as f_{γ}^{λ} (i.e the $HZ\gamma$ coupling) is small, the effects of it appear larger in $F_{\mathcal{B}7}$ than in $F_{\mathcal{C}8}$. Notice that this discussion is independent on explicit choices for λ and λ' . The above finding is true not only in $F_{\mathcal{B}7}$ but also in the other coefficients which have the overall σ in f_{ia} . These coefficients are indicated by the symbol \circ in the column " $HZ\gamma$ " in Table 3.

In Figure 6, the coefficients $F_{\mathcal{B}8}$ (left panel) and $F_{\mathcal{C}7}$ (right panel) divided by $F_{\mathcal{A}1}$ are shown in the same manner as Figure 5. $CP\widetilde{T}$ invariance requires these 2 coefficients to be identically zero, hence observation of a non-zero value indicates the existence of re-scattering effects. Re-scattering effects can be approximately included by allowing imaginary parts in the form factors [60]. In each panel, \square points give predictions for $h_3^Z = 0 + 0.1i$, and \times points give those for $h_3^\gamma = 0 + 0.1i$.

In Figure 7, the coefficients $F_{\mathcal{A}3}$ (left panel), $F_{\mathcal{D}1}$ (middle-left panel), $-F_{\mathcal{B}5}$ (middle-right panel) and $-F_{\mathcal{C}4}$ (right panel) divided by $F_{\mathcal{A}1}$ are shown in the same manner as Figure 5. These 4 coefficients are doubly constrained to be identically zero by CP invariance and $CP\tilde{T}$ invariance: they are strictly zero if CP is conserved, even if $CP\tilde{T}$ is violated, for instance. Observation of a non-zero value indicates CP violation and the existence of re-scattering effects. In each panel, \Box points give predictions for the CP-odd from factor $\tilde{h}_4^Z = 0 + 0.1i$, and \times points give those for the CP-odd form factor $\tilde{h}_4^{\gamma} = 0 + 0.1i$.

4 Polarisation of the W boson

In this section, we analyse the density matrices of the W^+ and W^- in the process $pp \to W^\pm H$ following the same procedure as Section 3. Because (1) a determination of the density matrix of the W boson is difficult in pp collisions when the W boson decays into a charged lepton and a neutrino and (2) we cannot distinguish W^+ from W^- in view of the difficulty of flavor identification of both W^+ and W^- decay products when the W boson decays into two quarks, we consider the process $pp \to W^\pm H$ ($W^\pm \to jj$) as the sum of the process $pp \to W^+ H$ ($W^+ \to jj$) and the process $pp \to W^- H$ ($W^- \to jj$). Just as the process $pp \to ZH$, only the 15 coefficients among the 36 coefficients of the 4 different differential angular distributions of the decay products can be non-zero. However only 9 coefficients among these 15 coefficients are actually measurable.

4.1 Polarisation density matrices of the W^+ and W^-

Fist of all, we define the density matrices of the W^+ and W^- . We consider the sub-processes

$$u(\sigma) + \bar{d}(-\sigma) \to W^{+}(\lambda) + H;$$

$$W^{+}(\lambda) \to u(\tau) + \bar{d}(-\tau), \tag{4.1a}$$

and

$$d(\sigma) + \bar{u}(-\sigma) \to W^{-}(\lambda) + H;$$

$$W^{-}(\lambda) \to d(\tau) + \bar{u}(-\tau), \tag{4.1b}$$

where the helicity of each particle is shown in parenthesis. We neglect the masses of the quark and the antiquark from the W decay, hence the helicity of the antiquark is always opposite to that of the quark. We prepare the 4 full helicity amplitudes $\mathcal{T}(u\bar{d})$, $\mathcal{T}(d\bar{u})$, $\mathcal{T}(\bar{d}u)$ and $\mathcal{T}(\bar{u}d)$ in which the production amplitude is evaluated in the $u\bar{d}$ c.m. frame, the $d\bar{u}$ c.m. frame, the $\bar{d}u$ c.m. frame and the $\bar{u}d$ c.m. frame, respectively. Recall that these c.m. frames are shown in Figure 3 and the production amplitudes are given in eqs. (2.8) and (2.9). These 4 full helicity amplitudes are given by

$$\mathcal{T}(u\bar{d}) = P_W \sum_{\lambda = +0} \mathcal{M}_{-}^{\lambda}(u\bar{d}) D_{\lambda}, \tag{4.2a}$$

$$\mathcal{T}(\bar{d}u) = P_W \sum_{\lambda = \pm .0} \mathcal{M}_{-}^{\lambda}(\bar{d}u) \ D_{\lambda}, \tag{4.2b}$$

$$\mathcal{T}(d\bar{u}) = P_W \sum_{\lambda = \pm, 0} \mathcal{M}_{-}^{\lambda}(d\bar{u}) \ \widetilde{D}_{\lambda}, \tag{4.2c}$$

$$\mathcal{T}(\bar{u}d) = P_W \sum_{\lambda = +.0} \mathcal{M}_{-}^{\lambda}(\bar{u}d) \ \tilde{D}_{\lambda}, \tag{4.2d}$$

where

$$P_W = (Q^2 - m_W^2 + im_W \Gamma_W)^{-1}$$
(4.3)

denotes the propagator factor of the W boson, D_{λ} is the helicity amplitude for the decay process $W^+ \to u\bar{d}$ and \widetilde{D}_{λ} is the helicity amplitude for the decay process $W^- \to d\bar{u}$:

$$D_{\lambda} = \frac{g}{\sqrt{2}} V_{ud} m_W \ d_{\lambda}^-, \tag{4.4a}$$

$$\widetilde{D}_{\lambda} = \frac{g}{\sqrt{2}} (V_{ud})^* m_W \ d_{\lambda}^-, \tag{4.4b}$$

where d_{λ}^{-} is given in eq. (3.6). The decay amplitudes are evaluated in the following four-momentum frame:

$$W^{+}(W^{-}): (m_{W}, 0, 0, 0)$$

$$u(d): \frac{m_{W}}{2} (1, \sin \widehat{\theta} \cos \widehat{\phi}, \sin \widehat{\theta} \sin \widehat{\phi}, \cos \widehat{\theta})$$

$$\bar{d}(\bar{u}): \frac{m_{W}}{2} (1, -\sin \widehat{\theta} \cos \widehat{\phi}, -\sin \widehat{\theta} \sin \widehat{\phi}, -\cos \widehat{\theta}). \tag{4.5}$$

Then we obtain

$$\left|\mathcal{T}(u\bar{d})\right|^{2} = \left|P_{W}m_{W}gV_{ud}/\sqrt{2}\right|^{2} \sum_{\lambda',\lambda} \left(d_{\lambda'}^{-}\right)^{*} \rho^{\lambda'\lambda}(u\bar{d}) \ d_{\lambda}^{-}, \tag{4.6a}$$

$$\left| \mathcal{T}(\bar{d}u) \right|^2 = \left| P_W m_W g V_{ud} / \sqrt{2} \right|^2 \sum_{\lambda', \lambda} \left(d_{\lambda'}^- \right)^* \rho^{\lambda' \lambda} (\bar{d}u) \ d_{\lambda}^-, \tag{4.6b}$$

$$\left|\mathcal{T}(d\bar{u})\right|^{2} = \left|P_{W}m_{W}gV_{ud}/\sqrt{2}\right|^{2} \sum_{\lambda',\lambda} \left(d_{\lambda'}^{-}\right)^{*} \rho^{\lambda'\lambda}(d\bar{u}) \ d_{\lambda}^{-}, \tag{4.6c}$$

$$\left| \mathcal{T}(\bar{u}d) \right|^2 = \left| P_W m_W g V_{ud} / \sqrt{2} \right|^2 \sum_{\lambda', \lambda} \left(d_{\lambda'}^- \right)^* \rho^{\lambda' \lambda}(\bar{u}d) \ d_{\lambda}^-, \tag{4.6d}$$

where

$$\rho^{\lambda'\lambda}(u\bar{d}) = \{\mathcal{M}_{-}^{\lambda'}(u\bar{d})\}^* \mathcal{M}_{-}^{\lambda}(u\bar{d}), \tag{4.7a}$$

$$\rho^{\lambda'\lambda}(\bar{d}u) = \left\{ \mathcal{M}_{-}^{\lambda'}(\bar{d}u) \right\}^* \mathcal{M}_{-}^{\lambda}(\bar{d}u), \tag{4.7b}$$

represent the elements of the density matrix in the helicity basis of the W^+ in the $u\bar{d}$ c.m. frame and those in the $\bar{d}u$ c.m. frame, respectively, and

$$\rho^{\lambda'\lambda}(d\bar{u}) = \left\{ \mathcal{M}_{-}^{\lambda'}(d\bar{u}) \right\}^* \mathcal{M}_{-}^{\lambda}(d\bar{u}), \tag{4.8a}$$

$$\rho^{\lambda'\lambda}(\bar{u}d) = \left\{ \mathcal{M}_{-}^{\lambda'}(\bar{u}d) \right\}^* \mathcal{M}_{-}^{\lambda}(\bar{u}d), \tag{4.8b}$$

represent the elements of the density matrix in the helicity basis of the W^- in the $d\bar{u}$ c.m. frame and those in the $\bar{u}d$ c.m. frame, respectively. By looking at the amplitudes in eqs. (2.8) and (2.9), it is easy to find the relations

$$\rho^{\lambda'\lambda}(u\bar{d}) = \rho^{\lambda'\lambda}(d\bar{u}),\tag{4.9a}$$

$$\rho^{\lambda'\lambda}(\bar{d}u) = \rho^{\lambda'\lambda}(\bar{u}d). \tag{4.9b}$$

The relations indicate that the W^+ and W^- are always in the same state of polarisation. This fact makes our analysis in the next section simpler, because we do not have to distinguish the W^+ from the W^- with regard to states of polarisation.

4.2 Decay angular distributions of the polarised W^+ and W^-

The complete differential cross section for the process $pp \to W^+H$ followed by $W^+ \to jj$ in the narrow width approximation can be expressed in terms of the density matrices in eq. (4.7) as

$$\begin{split} \frac{d\sigma^{W^{+}}}{d\hat{s} \; dy \; d\cos\theta \; d\cos\hat{\theta} \; d\hat{\phi}} = & \frac{m_{W}k}{8192\pi^{3}\Gamma_{W}s\hat{s}^{\frac{3}{2}}}g^{2} \Big(\sum_{u,d} \big|V_{ud}\big|^{2} \Big) \\ & \times \sum_{u,d} \bigg[u(x_{1})\bar{d}(x_{2}) \; d^{-\dagger}\rho(u\bar{d})d^{-} + \bar{d}(x_{1})u(x_{2}) \; d^{-\dagger}\rho(\bar{d}u)d^{-} \bigg], \end{split} \tag{4.10}$$

and that for the process $pp \to W^- H$ followed by $W^- \to jj$ can be expressed in terms of the density matrices in eq. (4.8) as

$$\begin{split} \frac{d\sigma^{W^{-}}}{d\hat{s} \; dy \; d\cos\theta \; d\cos\widehat{\theta} \; d\widehat{\phi}} = & \frac{m_W k}{8192\pi^3 \Gamma_W s \hat{s}^{\frac{3}{2}}} g^2 \Big(\sum_{u,d} \big| V_{ud} \big|^2 \Big) \\ & \times \sum_{u,d} \bigg[d(x_1) \bar{u}(x_2) \; d^{-\dagger} \rho(d\bar{u}) d^- + \bar{u}(x_1) d(x_2) \; d^{-\dagger} \rho(\bar{u}d) d^- \bigg], \end{split} \tag{4.11}$$

where the 3×3 matrix form in eq. (3.9) is used. For the definition of variables, see below eq. (3.12). As the quark flavors u and d summed in the above equations, we consider all the quark flavors but the top quark. As a result, the unitarity of the CKM matrix gives $\sum_{u,d} |V_{ud}|^2 = 2$. By using the relations in eq. (4.9), we obtain the complete differential cross section for the process $pp \to W^{\pm}H$

followed by $W^{\pm} \to jj$ as the sum of the above two cross sections in the following compact form:

$$\begin{split} \frac{d\sigma^{W^{+}+W^{-}}}{d\hat{s}\;dy\;d\cos\theta\;d\cos\hat{\theta}\;d\hat{\phi}} &= \frac{m_{W}k}{4096\pi^{3}\Gamma_{W}s\hat{s}^{\frac{3}{2}}}g^{2} \\ &\times \sum_{u,d} \left[\left\{ u(x_{1})\bar{d}(x_{2}) + d(x_{1})\bar{u}(x_{2}) \right\}\;d^{-\dagger}\rho(u\bar{d})d^{-} + \left\{ \bar{u}(x_{1})d(x_{2}) + \bar{d}(x_{1})u(x_{2}) \right\}\;d^{-\dagger}\rho(\bar{d}u)d^{-} \right]. \end{split} \tag{4.12}$$

As in Section 3.2, we derive the differential cross section with respect to \hat{s} , $\cos \hat{\theta}$ and $\hat{\phi}$ by integrating over y and $\cos \theta$ in eq. (4.12). It is straightforward to confirm that the integration over y and $\cos \theta$ in the 4 different approaches summarised in Table 1 can be performed in the same manner as eqs. (3.16), (3.18), (3.20) and (3.21). The resulting differential cross sections are

$$\begin{split} \frac{d\sigma^{W^++W^-}}{d\hat{s}\;d\cos\hat{\theta}\;d\hat{\phi}}\bigg|_{\mathcal{A}} &= \mathcal{T}^W \int_0^{y_{\rm cut}} dy\; 2\Big[u(x_1)\bar{d}(x_2) + d(x_1)\bar{u}(x_2) + \bar{u}(x_1)d(x_2) + \bar{d}(x_1)u(x_2)\Big] \\ &\times d^{-\dagger} \begin{pmatrix} c_1|\hat{N}^+|^2 & \frac{1}{2}c_2(\hat{N}^+)^*\hat{N}^- & 0\\ \frac{1}{2}c_2\hat{N}^+(\hat{N}^-)^* & c_1|\hat{N}^-|^2 & 0\\ 0 & 0 & c_2|\hat{N}^0|^2 \end{pmatrix} d^-, \quad (4.13a) \\ \frac{d\sigma^{W^++W^-}}{d\hat{s}\;d\cos\hat{\theta}\;d\hat{\phi}}\bigg|_{\mathcal{B}} &= \mathcal{T}^W \int_0^{y_{\rm cut}} dy\; 2\Big[u(x_1)\bar{d}(x_2) + d(x_1)\bar{u}(x_2) - \bar{u}(x_1)d(x_2) - \bar{d}(x_1)u(x_2)\Big] \\ &\times d^{-\dagger} \begin{pmatrix} 0 & 0 & -c_3(\hat{N}^+)^*\hat{N}^0\\ 0 & 0 & -c_3(\hat{N}^-)^*\hat{N}^0 \end{pmatrix} d^-, \quad (4.13b) \\ \frac{d\sigma^{W^++W^-}}{d\hat{s}\;d\cos\hat{\theta}\;d\hat{\phi}}\bigg|_{\mathcal{C}} &= \mathcal{T}^W \int_0^{y_{\rm cut}} dy\; 2\Big[u(x_1)\bar{d}(x_2) + d(x_1)\bar{u}(x_2) + \bar{u}(x_1)d(x_2) + \bar{d}(x_1)u(x_2)\Big] \\ &\times d^{-\dagger} \begin{pmatrix} 0 & 0 & c_4(\hat{N}^+)^*\hat{N}^0\\ 0 & 0 & -c_4(\hat{N}^-)^*\hat{N}^0 \end{pmatrix} d^-, \quad (4.13c) \\ c_4\hat{N}^+(\hat{N}^0)^* & -c_4\hat{N}^-(\hat{N}^0)^* & 0 \end{pmatrix} d^-, \quad (4.13c) \\ \frac{d\sigma^{W^++W^-}}{d\hat{s}\;d\cos\hat{\theta}\;d\hat{\phi}}\bigg|_{\mathcal{D}} &= \mathcal{T}^W \int_0^{y_{\rm cut}} dy\; 2\Big[u(x_1)\bar{d}(x_2) + d(x_1)\bar{u}(x_2) - \bar{u}(x_1)d(x_2) - \bar{d}(x_1)u(x_2)\Big] \\ &\times d^{-\dagger} \begin{pmatrix} -c_5|\hat{N}^+|^2 & 0 & 0\\ 0 & c_5|\hat{N}^-|^2 & 0\\ 0 & 0 & 0 \end{pmatrix} d^-, \quad (4.13d) \end{split}$$

where

$$\mathcal{T}^{W} = \frac{m_{W}k}{4096\pi^{3}\Gamma_{W}s\hat{s}^{\frac{3}{2}}}g^{2}\sum_{u,d}\left|V_{ud}\right|^{2},\tag{4.14}$$

the constant values c_i (i=1,2,3,4,5) are summarised in Table 2, and $\hat{N}^{\lambda=\pm,0}$ are defined in eq. (2.10). By comparing the above 4 differential cross sections with eq. (3.22), we obtain the 36 coefficients F_{ia}^W $(i=\mathcal{A},\mathcal{B},\mathcal{C},\mathcal{D})$ $(a=1,2,\cdots,9)$ in total:

$$F_{\mathcal{A}(\mathcal{C})a}^{W} = \mathcal{T}^{W} \int_{0}^{y_{\text{cut}}} dy \ 2 \left[u(x_{1})\bar{d}(x_{2}) + d(x_{1})\bar{u}(x_{2}) + \bar{u}(x_{1})d(x_{2}) + \bar{d}(x_{1})u(x_{2}) \right] f_{\mathcal{A}(\mathcal{C})a}^{W}, \quad (4.15a)$$

$$F_{\mathcal{B}(\mathcal{D})a}^{W} = \mathcal{T}^{W} \int_{0}^{y_{\text{cut}}} dy \ 2 \left[u(x_{1})\bar{d}(x_{2}) + d(x_{1})\bar{u}(x_{2}) - \bar{u}(x_{1})d(x_{2}) - \bar{d}(x_{1})u(x_{2}) \right] f_{\mathcal{B}(\mathcal{D})a}^{W}, \quad (4.15b)$$

where f_{ia}^W $(i = \mathcal{A}, \mathcal{B}, \mathcal{C}, \mathcal{D})$ $(a = 1, 2, \dots, 9)$ are obtained by the following replacements in those coefficients of the process $pp \to ZH$ in eq. (3.24):

$$\hat{M}^{\lambda}_{\sigma} \to \hat{N}^{\lambda}, \quad \sigma \to -1, \quad \tau \to -1.$$
 (4.16)

Table 3 corresponding to the process $pp \to W^{\pm}H$ is obtained by the following simple replacements in Table 3:

$$\hat{M}^{\lambda}_{\sigma} \to \hat{N}^{\lambda}, \quad F_{ia} \to F^{W}_{ia}.$$
 (4.17)

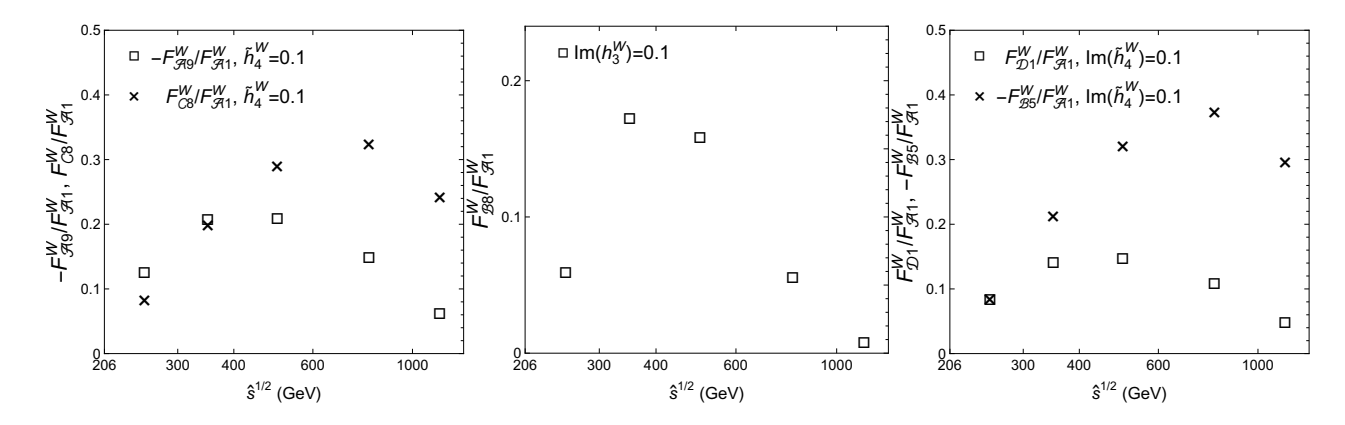


Figure 8: In the left panel, the 2 coefficients $-F_{\mathcal{A}9}^W$ (\square) and $F_{\mathcal{C}8}^W$ (\times) divided by $F_{\mathcal{A}1}^W$ are shown for $\tilde{h}_4^W=0.1$. These 2 coefficients are constrained to be identically zero by CP invariance. In the middle panel, the coefficient $F_{\mathcal{B}8}^W$ divided by $F_{\mathcal{A}1}^W$ are shown for $h_3^W=0+0.1i$. This coefficient is constrained to be identically zero by CPT invariance. In the right panel, the 2 coefficients $F_{\mathcal{D}1}^W$ (\square) and $-F_{\mathcal{B}5}^W$ (\times) divided by $F_{\mathcal{A}1}^W$ are shown for $\tilde{h}_4^W=0+0.1i$. These 2 coefficients are doubly constrained to be identically zero by CP invariance and CPT invariance. For each result, the values in the 5 bins, from left to right, are obtained after integration over \hat{s} in the regions $(m_W+m_H)<\hat{s}^{1/2}<300$, $300<\hat{s}^{1/2}<400$, $400<\hat{s}^{1/2}<600$, $600<\hat{s}^{1/2}<1000$ and $1000<\hat{s}^{1/2}<14000$ in units of GeV.

Just as the process $pp \to ZH$, there are in total 15 coefficients which can be non-zero. Observation of the 6 coefficients $F_{\mathcal{D}3}^W$, $F_{\mathcal{A}3}^W$, $F_{\mathcal{B}4}^W$, $F_{\mathcal{C}4}^W$, $F_{\mathcal{B}7}^W$ and $F_{\mathcal{C}7}^W$ has difficulty, since it requires the charge (or flavor) identification of the parent quark of the jet. Only the remaining 9 coefficients $F_{\mathcal{A}1}^W$, $F_{\mathcal{A}2}^W$, $F_{\mathcal{D}1}^W$, $F_{\mathcal{C}5}^W$, $F_{\mathcal{B}5}^W$, $F_{\mathcal{B}6}^W$, $F_{\mathcal{B}8}^W$ and $F_{\mathcal{A}9}^W$ are, therefore, actually measurable. We emphasise that these 9 coefficients are necessary and sufficient to determine all of the 9 independent combinations of the polarisation density matrix elements.

4.3 Influences of non-standard HWW interaction

In this Section, with the same motivation as Section 3.3, we focus on the measurable coefficients which are strictly zero or small in the SM, and study the influences of the non-standard HWW coupling. In the left panel of Figure 8, the 2 coefficients $-F_{A9}^W$ (\square) and F_{C8}^W (\times) divided by F_{A1}^W are shown for the CP-odd form factor $\tilde{h}_4^W=0.1$. CP invariance requires these 2 coefficients to be identically zero; observation of a non-zero value signals CP violation. In the middle panel of Figure 8, the coefficient F_{B8}^W divided by F_{A1}^W is shown for the CP-even form factor $h_3^W=0+0.1i$. $CP\tilde{T}$ invariance requires this coefficient to be identically zero; observation of a non-zero value indicates the existence of re-scattering effects. In the right panel of Figure 8, the 2 coefficients F_{D1}^W (\square) and $-F_{B5}^W$ (\times) divided by F_{A1}^W are shown for the CP-odd form factor $\tilde{h}_4^W=0+0.1i$. These 2 coefficients are doubly constrained to be identically zero by CP invariance and $CP\tilde{T}$ invariance; observation of a non-zero value indicates CP violation and the existence of re-scattering effects. For each result, the values in the 5 bins, from left to right, are obtained after integration over \hat{s} in the regions $(m_W+m_H)<\hat{s}^{1/2}<300$, $300<\hat{s}^{1/2}<400$, $400<\hat{s}^{1/2}<600$, $600<\hat{s}^{1/2}<1000$ and $1000<\hat{s}^{1/2}<14000$ in units of GeV.

We discuss the differences between the coefficients F_{ia} in the process $pp \to ZH$ and those F_{ia}^W in the process $pp \to W^\pm H$. From the comparisons between the results for the non-standard HZZ coupling in Figures 5, 6 and 7 and the results for the non-standard HWW coupling in Figure 8, we notice that F_{A9}^W and F_{C8}^W are comparable with F_{A9} and F_{C8} , respectively, while F_{B8}^W , F_{D1}^W and F_{B5}^W are consistently larger than F_{B8} , F_{D1} and F_{B5} , respectively. As we have discussed at the last paragraph of Section 2.2, the Z boson is in a partially polarised state, while the W^+ and W^- are in a completely polarised state. The degree of polarisation affects the magnitudes of the coefficients, hence it is expected that the coefficients F_{ia}^W are always equal or larger than the coefficients F_{ia} . The existence of the overall σ in F_{B8} , F_{D1} and F_{B5} (see eq. (3.24)) indicates that these coefficients are weakened according to the degree of polarisation of the Z boson. These coefficients are denoted by the symbol \circ in the last column in Table 3.

5 Summary

The measurements of the Higgs boson couplings to the SM particles are essential tests of the SM. The Z boson in the process $pp \to ZH$ and the W^+ and W^- in the process $pp \to W^\pm H$ can be in polarised states, and it would be possible to study the Higgs boson couplings to the weak bosons $(HZZ, HZ\gamma)$ and HWW in detail from a careful analysis of these states of polarisation. A density matrix contains the complete information about a state of polarisation, and all of the elements of the density matrix should be made use of in such a careful analysis. In this paper, such an analysis approach has been presented.

Determination of the density matrix of the Z(W) boson requires measurements of the angular distributions of the Z(W) decay products. In pp collisions, this is difficult when the W boson decays into a charged lepton and a neutrino. When the W boson decays into two quarks, we cannot distinguish W^+ from W^- in view of the difficulty of flavor identification of both W^+ and W^- decay products. Therefore, we have considered the process $pp \to W^\pm H$ ($W^\pm \to jj$) as the sum of the process $pp \to W^+H$ ($W^+ \to jj$) and the process $pp \to W^-H$ ($W^- \to jj$). We have found that the W^+ and W^- are always in the same state of polarisation (i.e. the density matrix of the W^+ is always the same as that of W^-). By using this fact, we have developed a analysis approach which can be applied both to the $pp \to ZH$ ($Z \to f\bar{f}$) and to the $pp \to W^\pm H$ ($W^\pm \to jj$) in the same manner.

We have derived the 4 different differential cross sections with respect to \hat{s} (the invariant mass squared of the Z(W) boson and the Higgs boson) and $\cos \hat{\theta}$ and $\hat{\phi}$ (the Z(W) decay angles), by integrating the complete differential cross section over the other phase space variables in the 4 different approaches. Among the 36 coefficients (= 9×4) of these 4 differential angular distributions, only 15 coefficients can be non-zero (these coefficients are summarised in Table 3). These 15 coefficients are written in terms of the elements of the density matrices, and there exist 9 independent combinations of the elements of the density matrices. Observation of the 9 coefficients among the 15 coefficients does not require the charge (or flavor) identification of the Z(W) decay products. In the analysis of the W^+ and W^- , only these 9 coefficients are measurable. We have found that these 9 coefficients are necessary and sufficient to determine all of the 9 independent combinations of the density matrix elements (i.e. one coefficient corresponds to one combination). We have clarified the restrictions on the 15 coefficients imposed by the CP and $CP\widetilde{T}$ symmetries. Some of the coefficients are required to be identically zero by CPinvariance; observation of a non-zero value in these coefficients signals CP violation. Similarly, some of the coefficients are required to be identically zero by $CP\widetilde{T}$ invariance; observation of a non-zero value in these coefficients indicates the existence of re-scattering effects. These coefficients are in particular interesting as observables at the LHC, since observation of a non-zero or large value in these coefficients immediately signals the existence of non-standard HZZ, $HZ\gamma$ and/or HWW interactions.

Acknowledgments

I would like to thank Kaoru Hagiwara for many discussions. I am also grateful to members of CP3, Université Catholique de Louvain for their hospitality. My work is supported by the Alexander von Humboldt Foundation.

References

- [1] ATLAS collaboration, G. Aad et al., Observation of a new particle in the search for the Standard Model Higgs boson with the ATLAS detector at the LHC, Phys. Lett. B716 (2012) 1–29, [1207.7214].
- [2] CMS collaboration, S. Chatrchyan et al., Observation of a new boson at a mass of 125 GeV with the CMS experiment at the LHC, Phys. Lett. B716 (2012) 30-61, [1207.7235].
- [3] LHC Higgs Cross Section Working Group collaboration, J. R. Andersen et al., *Handbook of LHC Higgs Cross Sections: 3. Higgs Properties*, 1307.1347.
- [4] J. R. Dell'Aquila and C. A. Nelson, P or CP Determination by Sequential Decays: V1 V2 Modes With Decays Into $\bar{\ell}$ epton (A) $\ell(B)$ And/or \bar{q} (A) q(B), Phys. Rev. **D33** (1986) 80.
- [5] C. A. Nelson, Correlation Between Decay Planes in Higgs Boson Decays Into W Pair (Into Z Pair), Phys. Rev. D37 (1988) 1220.

- [6] V. D. Barger, K.-m. Cheung, A. Djouadi, B. A. Kniehl and P. M. Zerwas, Higgs bosons: Intermediate mass range at e+ e- colliders, Phys. Rev. D49 (1994) 79–90, [hep-ph/9306270].
- [7] M. Kramer, J. H. Kuhn, M. L. Stong and P. M. Zerwas, Prospects of measuring the parity of Higgs particles, Z. Phys. C64 (1994) 21–30, [hep-ph/9404280].
- [8] S. Y. Choi, D. J. Miller, M. M. Muhlleitner and P. M. Zerwas, *Identifying the Higgs spin and parity in decays to Z pairs*, *Phys. Lett.* **B553** (2003) 61–71, [hep-ph/0210077].
- [9] C. P. Buszello, I. Fleck, P. Marquard and J. J. van der Bij, Prospective analysis of spin- and CP-sensitive variables in $H -_{\dot{c}} Z Z -_{\dot{c}} l(1) + l(1) l(2) + l(2)$ at the LHC, Eur. Phys. J. C32 (2004) 209–219, [hep-ph/0212396].
- [10] K. Hagiwara, Q. Li and K. Mawatari, Jet angular correlation in vector-boson fusion processes at hadron colliders, JHEP 07 (2009) 101, [0905.4314].
- [11] Y. Gao, A. V. Gritsan, Z. Guo, K. Melnikov, M. Schulze and N. V. Tran, Spin determination of single-produced resonances at hadron colliders, Phys. Rev. D81 (2010) 075022, [1001.3396].
- [12] S. Bolognesi, Y. Gao, A. V. Gritsan, K. Melnikov, M. Schulze, N. V. Tran et al., On the spin and parity of a single-produced resonance at the LHC, Phys. Rev. D86 (2012) 095031, [1208.4018].
- [13] T. Plehn, D. L. Rainwater and D. Zeppenfeld, Determining the structure of Higgs couplings at the LHC, Phys. Rev. Lett. 88 (2002) 051801, [hep-ph/0105325].
- [14] V. Hankele, G. Klamke, D. Zeppenfeld and T. Figy, Anomalous Higgs boson couplings in vector boson fusion at the CERN LHC, Phys. Rev. D74 (2006) 095001, [hep-ph/0609075].
- [15] C. Englert, D. Goncalves-Netto, K. Mawatari and T. Plehn, Higgs Quantum Numbers in Weak Boson Fusion, JHEP 01 (2013) 148, [1212.0843].
- [16] J. Nakamura and J. Baglio, Jet azimuthal angle correlations in the production of a Higgs boson pair plus two jets at hadron colliders, Eur. Phys. J. C77 (2017) 35, [1603.02315].
- [17] ATLAS collaboration, G. Aad et al., Measurements of Higgs boson production and couplings in diboson final states with the ATLAS detector at the LHC, Phys. Lett. B726 (2013) 88–119, [1307.1427].
- [18] ATLAS collaboration, G. Aad et al., Measurements of Higgs boson production and couplings in the four-lepton channel in pp collisions at center-of-mass energies of 7 and 8 TeV with the ATLAS detector, Phys. Rev. D91 (2015) 012006, [1408.5191].
- [19] ATLAS collaboration, G. Aad et al., Measurements of the Higgs boson production and decay rates and coupling strengths using pp collision data at $\sqrt{s} = 7$ and 8 TeV in the ATLAS experiment, Eur. Phys. J. C76 (2016) 6, [1507.04548].
- [20] ATLAS collaboration, G. Aad et al., Study of (W/Z)H production and Higgs boson couplings using $H \to WW^*$ decays with the ATLAS detector, JHEP **08** (2015) 137, [1506.06641].
- [21] ATLAS, CMS collaboration, G. Aad et al., Measurements of the Higgs boson production and decay rates and constraints on its couplings from a combined ATLAS and CMS analysis of the LHC pp collision data at $\sqrt{s} = 7$ and 8 TeV, JHEP **08** (2016) 045, [1606.02266].
- [22] CMS collaboration, S. Chatrchyan et al., Measurement of Higgs boson production and properties in the WW decay channel with leptonic final states, JHEP 01 (2014) 096, [1312.1129].
- [23] CMS collaboration, V. Khachatryan et al., Observation of the diphoton decay of the Higgs boson and measurement of its properties, Eur. Phys. J. C74 (2014) 3076, [1407.0558].
- [24] CMS collaboration, V. Khachatryan et al., Precise determination of the mass of the Higgs boson and tests of compatibility of its couplings with the standard model predictions using proton collisions at 7 and 8 TeV, Eur. Phys. J. C75 (2015) 212, [1412.8662].
- [25] ATLAS collaboration, G. Aad et al., Evidence for the spin-0 nature of the Higgs boson using ATLAS data, Phys. Lett. B726 (2013) 120–144, [1307.1432].
- [26] ATLAS collaboration, G. Aad et al., Determination of spin and parity of the Higgs boson in the WW* → eνμν decay channel with the ATLAS detector, Eur. Phys. J. C75 (2015) 231, [1503.03643].
- [27] ATLAS collaboration, G. Aad et al., Study of the spin and parity of the Higgs boson in diboson decays with the ATLAS detector, Eur. Phys. J. C75 (2015) 476, [1506.05669].
- [28] CMS collaboration, S. Chatrchyan et al., Study of the Mass and Spin-Parity of the Higgs Boson Candidate Via Its Decays to Z Boson Pairs, Phys. Rev. Lett. 110 (2013) 081803, [1212.6639].
- [29] CMS collaboration, S. Chatrchyan et al., Measurement of the properties of a Higgs boson in the four-lepton final state, Phys. Rev. D89 (2014) 092007, [1312.5353].
- [30] CMS collaboration, V. Khachatryan et al., Constraints on the spin-parity and anomalous HVV couplings of the Higgs boson in proton collisions at 7 and 8 TeV, Phys. Rev. D92 (2015) 012004, [1411.3441].

- [31] ATLAS collaboration, G. Aad et al., Constraints on non-Standard Model Higgs boson interactions in an effective Lagrangian using differential cross sections measured in the $H \to \gamma \gamma$ decay channel at $\sqrt{s} = 8 \, \text{TeV}$ with the ATLAS detector, Phys. Lett. B753 (2016) 69–85, [1508.02507].
- [32] ATLAS collaboration, G. Aad et al., Test of CP Invariance in vector-boson fusion production of the Higgs boson using the Optimal Observable method in the ditau decay channel with the ATLAS detector, Eur. Phys. J. C76 (2016) 658, [1602.04516].
- [33] CMS collaboration, V. Khachatryan et al., Combined search for anomalous pseudoscalar HVV couplings in $VH(H \to b\bar{b})$ production and $H \to VV$ decay, Phys. Lett. **B759** (2016) 672–696, [1602.04305].
- [34] S. L. Glashow, D. V. Nanopoulos and A. Yildiz, Associated Production of Higgs Bosons and Z Particles, Phys. Rev. D18 (1978) 1724–1727.
- [35] V. D. Barger, E. W. N. Glover, K. Hikasa, W.-Y. Keung, M. G. Olsson, C. J. Suchyta et al., Higgs Boson Z⁰ Associated Production From Fourth Generation Quarks at Super Collider Energies, Phys. Rev. Lett. 57 (1986) 1672.
- [36] B. A. Kniehl, Associated Production of Higgs and Z Bosons From Gluon Fusion in Hadron Collisions, Phys. Rev. D42 (1990) 2253–2258.
- [37] T. Han and S. Willenbrock, Qcd correction to the pp wh and zh total cross sections, Physics Letters B 273 (1991) 167 172.
- [38] J. Ohnemus and W. J. Stirling, Order alpha-s corrections to the differential cross-section for the W H intermediate mass Higgs signal, Phys. Rev. D47 (1993) 2722–2729.
- [39] M. L. Ciccolini, S. Dittmaier and M. Kramer, Electroweak radiative corrections to associated WH and ZH production at hadron colliders, Phys. Rev. D68 (2003) 073003, [hep-ph/0306234].
- [40] O. Brein, A. Djouadi and R. Harlander, NNLO QCD corrections to the Higgs-strahlung processes at hadron colliders, Phys. Lett. B579 (2004) 149–156, [hep-ph/0307206].
- [41] G. Ferrera, M. Grazzini and F. Tramontano, Associated WH production at hadron colliders: a fully exclusive QCD calculation at NNLO, Phys. Rev. Lett. 107 (2011) 152003, [1107.1164].
- [42] O. Brein, R. Harlander, M. Wiesemann and T. Zirke, Top-Quark Mediated Effects in Hadronic Higgs-Strahlung, Eur. Phys. J. C72 (2012) 1868, [1111.0761].
- [43] A. Denner, S. Dittmaier, S. Kallweit and A. Muck, Electroweak corrections to Higgs-strahlung off W/Z bosons at the Tevatron and the LHC with HAWK, JHEP 03 (2012) 075, [1112.5142].
- [44] S. Dawson, T. Han, W. K. Lai, A. K. Leibovich and I. Lewis, Resummation Effects in Vector-Boson and Higgs Associated Production, Phys. Rev. D86 (2012) 074007, [1207.4207].
- [45] L. Altenkamp, S. Dittmaier, R. V. Harlander, H. Rzehak and T. J. E. Zirke, Gluon-induced Higgs-strahlung at next-to-leading order QCD, JHEP 02 (2013) 078, [1211.5015].
- [46] O. Brein, R. V. Harlander and T. J. E. Zirke, vh@nnlo Higgs Strahlung at hadron colliders, Comput. Phys. Commun. 184 (2013) 998–1003, [1210.5347].
- [47] N. D. Christensen, T. Han and Y. Li, Testing CP Violation in ZZH Interactions at the LHC, Phys. Lett. B693 (2010) 28–35, [1005.5393].
- [48] N. Desai, D. K. Ghosh and B. Mukhopadhyaya, CP-violating HWW couplings at the Large Hadron Collider, Phys. Rev. D83 (2011) 113004, [1104.3327].
- [49] R. Godbole, D. J. Miller, K. Mohan and C. D. White, Boosting Higgs CP properties via VH Production at the Large Hadron Collider, Phys. Lett. B730 (2014) 275–279, [1306.2573].
- [50] C. Delaunay, G. Perez, H. de Sandes and W. Skiba, Higgs Up-Down CP Asymmetry at the LHC, Phys. Rev. D89 (2014) 035004, [1308.4930].
- [51] F. Maltoni, K. Mawatari and M. Zaro, Higgs characterisation via vector-boson fusion and associated production: NLO and parton-shower effects, Eur. Phys. J. C74 (2014) 2710, [1311.1829].
- [52] I. Anderson et al., Constraining anomalous HVV interactions at proton and lepton colliders, Phys. Rev. D89 (2014) 035007, [1309.4819].
- [53] R. M. Godbole, D. J. Miller, K. A. Mohan and C. D. White, Jet substructure and probes of CP violation in Vh production, JHEP 04 (2015) 103, [1409.5449].
- [54] S. Dwivedi, D. K. Ghosh, B. Mukhopadhyaya and A. Shivaji, Distinguishing CP-odd couplings of the Higgs boson to weak boson pairs, Phys. Rev. D93 (2016) 115039, [1603.06195].
- [55] F. Ferreira, B. Fuks, V. Sanz and D. Sengupta, Probing CP-violating Higgs and gauge boson couplings in the Standard Model effective field theory, 1612.01808.
- [56] L. D. Landau and E. M. Lifshitz, Quantum Mechanics Non-relativistic Theory, Course of Theoretical Physics Volume 3, Third edition, Butterworth Heinemann (1977).
- [57] L. I. Schiff, quantum mechanics, third edition, McGraw-Hill (1968).

- [58] C. Bourrely, E. Leader and J. Soffer, *Polarization phenomena in hadronic reactions*, *Physics Reports* **59** (1980) 95 297.
- [59] N. S. Craigie, K. Hidaka, M. Jacob and F. M. Renard, Spin Physics at Short Distances, Phys. Rept. 99 (1983) 69–236.
- [60] K. Hagiwara, R. D. Peccei, D. Zeppenfeld and K. Hikasa, Probing the Weak Boson Sector in $e^+e^- \to W^+W^-$, Nucl. Phys. **B282** (1987) 253–307.
- [61] OPAL collaboration, G. Abbiendi et al., Measurement of W boson polarizations and CP violating triple gauge couplings from W⁺W⁻ production at LEP, Eur. Phys. J. C19 (2001) 229–240, [hep-ex/0009021].
- [62] OPAL collaboration, G. Abbiendi et al., W boson polarization at LEP2, Phys. Lett. B585 (2004) 223-236, [hep-ex/0312047].
- [63] DELPHI collaboration, J. Abdallah et al., Study of W boson polarisations and Triple Gauge boson Couplings in the reaction $e^+e^- \rightarrow W^+W^-$ at LEP 2, Eur. Phys. J. C54 (2008) 345–364, [0801.1235].
- [64] R. L. Kelly and T. Shimada, Dilepton Signature in $e^+e^- \to H\ell^+\ell^-$, Phys. Rev. **D23** (1981) 1940.
- [65] R. Rattazzi, Anomalous Interactions at the Z⁰ Pole, Z. Phys. C40 (1988) 605–611.
- [66] K. Hagiwara and M. L. Stong, Probing the scalar sector in e+ e- -- ¿ f anti-f H, Z. Phys. C62 (1994) 99–108, [hep-ph/9309248].
- [67] K. Hagiwara, S. Ishihara, J. Kamoshita and B. A. Kniehl, Prospects of measuring general Higgs couplings at e+ e- linear colliders, Eur. Phys. J. C14 (2000) 457–468, [hep-ph/0002043].
- [68] D. Binosi and L. Theussl, JaxoDraw: A Graphical user interface for drawing Feynman diagrams, Comput. Phys. Commun. 161 (2004) 76–86, [hep-ph/0309015].
- [69] M. Kobayashi and T. Maskawa, CP Violation in the Renormalizable Theory of Weak Interaction, Prog. Theor. Phys. 49 (1973) 652–657.
- [70] A. D. Martin, W. J. Stirling, R. S. Thorne and G. Watt, Parton distributions for the LHC, Eur. Phys. J. C63 (2009) 189–285, [0901.0002].
- [71] S. Kawabata, A New version of the multidimensional integration and event generation package BASES/SPRING, Comput. Phys. Commun. 88 (1995) 309–326.